The short-chain fatty acid butyrate prevents gut-brain amyloid-β pathology and neuroinflammation in an Alzheimer mouse model

Rodrigue Brossaud, Thibauld Oullier, Anne Bessard, Philippe Aubert, Lisa Brossard, Maxime Mahé, Martial Caillaud, Giada Delfino, Sebastien Paillusson, Hélène Falentin, et al.

ARTICLE OPEN

Check for updates

The short-chain fatty acid butyrate prevents gut-brain amyloid-β pathology and neuroinflammation in an Alzheimer mouse model

Rodrigue Brossaud[1], Thibauld Oullier[1], Anne Bessard[1], Philippe Aubert[1], Lisa Brossard[1], Maxime M. Mahé[1], Martial Caillaud[1], Giada Delfino[1], Sebastien Paillusson[1], Hélène Falentin[2], Philippe Naveilhan[1], Yves Le-Loir[3], Vincent Paillé[3], Michel Neunlist[1] and Moustapha Cissé[1]✉

Amyloid-β (Aβ) plays a critical role in Alzheimer's disease (AD) and its accumulation in the brain is pivotal to disease progression and precedes memory and neuronal loss. Besides the severely handicapping brain symptoms, AD patients display early gastro-intestinal (GI) manifestations such as upper and lower GI dysmotility, in particular constipation. Although there is increasing evidence of Aβ accumulation in the gut, its pathogenic effects on enteric nervous system (ENS) connectivity and gut function as well as underlying pathophysiological mechanisms are poorly understood. Furthermore, studies have reported a gut to brain transmission of Aβ that causes memory deficits in mice. Therefore, identifying therapeutics which can reduce Aβ accumulation in the gut at an early stage of the disease could have the advantage of slowing or even reversing disease progression before severe alterations or irreversible damages at both intestinal and brain levels. Hence, in this study, we investigated the capacity of the short-fatty acid butyrate to restore Aβ-driven alteration of ENS connectivity and gut-brain functions in the SAMP8 mouse model of AD. Here we show that SAMP8 mice display a gut amyloid pathology, an alteration of ENS connectivity and gut defects prior to memory decline. BACE1, an Aβ-producing enzyme, expression and activity are increased whereas neprilysin, an Aβ-degrading enzyme, is decreased in the gut of SAMP8 mice, indicating a rise in the Amyloid Precursor Protein (APP) holoprotein processing and a reduction of Aβ clearance which promote an amyloidosis. In primary ENS cultures, Aβ causes a degradation of synaptic-associated proteins EphB2 and synaptophysin, leading to an alteration of ENS connectivity. In wild-type mice, intra-colon delivery of Aβ alters ENS connectivity and causes subsequent GI symptoms, recapitulating the phenotype of the SAMP8 mouse model of aging and AD. Moreover, Aβ impairs ENS connectivity in human induced pluripotent stem cell (iPSC)-derived intestinal organoids and explant cultures of human colon, indicating that Aβ causes ENS lesions in models of the human gut. Butyrate, a short-chain fatty acid derived from bacterial metabolism, reduces Aβ secretion and preserves enteric neuronal connectivity in vitro and in vivo, and blocks Aβ accumulation in the gut, brain and plasma in SAMP8 mice. In addition, butyrate ameliorates neuroinflammation and prevents gut dysfunction and memory deficit. Collectively, these findings suggest that Aβ promotes gut symptoms through alteration of ENS connectivity and butyrate counteracts these impairments with an amelioration of neuroinflammation and memory function in AD model.

Molecular Psychiatry; https://doi.org/10.1038/s41380-026-03522-6

INTRODUCTION

Alzheimer's disease (AD) is a progressive neurodegenerative disease mostly associated with cognitive decline and has no effective treatment to date. A major histological hallmark of AD pathogenesis is the formation of amyloid plaques caused by deposition of the amyloid-β (Aβ) peptide, which is produced by the proteolytic cleavage by β- and γ-secretase activities of amyloid precursor protein (APP) holoprotein that localizes to the plasma membrane [1]. Besides cognitive deficits, Alzheimer's patients often suffer from other comorbidities [2, 3], including gastro-intestinal (GI) symptoms, such as upper and lower bowel dysmotility, in particular constipation, which have recently drawn attention due to early manifestations, sometimes decades before memory loss [4]. Interestingly, recent studies indicate that patients with constipation are at greater risk of developing AD [5] and are more likely to display a faster progression of brain symptoms [6]. Similarly to Parkinson's disease [7], these findings support a change in the long-held dogma that AD is a brain centered disease and an evolution towards a more complex notion of a multi-organ disease, in which peripheric organs, in particular the gut, play a pivotal role [8]. Therefore, better understanding AD-associated pathophysiological mechanisms and identifying

[1]Nantes Université, CHU Nantes, INSERM, The enteric nervous system in gut and brain disorders, IMAD, F-44000 Nantes, France. [2]Science et Technique du Lait et de l'Œuf, Institut National de Recherche pour l'Agriculture, l'Alimentation et l'Environnement (INRAE), Unité Mixte de Recherche, L'Institut Agro, F-35042 Rennes, France. [3]Nantes Université, CHU Nantes, INRAE, UMR 1280, PhAN, IMAD, F-44000 Nantes, France. ✉email: moustapha.cisse@univ-nantes.fr

Received: 26 August 2025 Revised: 23 January 2026 Accepted: 18 February 2026
Published online: 05 March 2026

therapeutic strategies to restore gut functions and memory in AD, although fraught with challenges, would constitute a significant step forward in AD research. Thus, the gut represents not only an organ to better understand AD pathophysiology, but also a therapeutic target to ameliorate GI symptoms.

The enteric nervous system (ENS), a critical regulator of gut functions [9], is likely involved in GI symptoms in AD [10]. Previous studies indicate that Aβ accumulates in the gut of AD mice and patients with AD [11, 12]. Because Aβ affects brain plasticity to cause memory deficits [13], it might also alter gut connectivity to cause GI symptoms. In the brain, Aβ interacts functionally and structurally with several distinct types of plasma membrane–anchored receptors, including EphB2 receptor tyrosine kinase, a master regulator of neuronal plasticity [14, 15]. We have recently shown that EphB2 receptor is an important regulator of ENS connectivity [16]. Whether Aβ harms enteric neurons in a similar fashion to neurons in the brain by impairing synaptic proteins such as EphB2 remains to be established. Furthermore, whether alterations of ENS connectivity and GI dysfunction can be prevented through pharmacological intervention in AD context is unknown.

The short chain fatty acid (SCFA) butyrate is a natural product of bacterial fermentation of dietary fiber in the colon [17], a major source of energy for colonocytes. It also exerts beneficial effects via the maintenance of intestinal epithelium barrier integrity, gut motility and anti-inflammatory effects. In addition, butyrate has also the capacity to regulate central nervous system (CNS) functions such as the blood brain barrier and has been shown to protect against Aβ toxicity to CNS neurons both in vitro [18] and in vivo [19, 20]. However, butyrate capacity to counteract amyloid pathology in the gut and in particular its toxicity in the ENS remains unexplored in AD.

Here, we performed a longitudinal characterization of gut and brain functions in the SAMP8 model of aging and sporadic AD. We explored gut amyloidogenesis in early stages, prior to memory deficit. We examined ENS connectivity and measured APP amyloidogenic processing, Aβ levels and clearance. Furthermore, we investigated the causal role of Aβ in ENS lesions and GI dysfunction in different in vitro and in vivo models, including ENS cultures, iPSC-derived intestinal organoids, human colon explants and mice by using electrophysiology, imaging, biochemistry, gut function exploration and behavior. Finally, we explored butyrate capacity to block Aβ-driven ENS lesions and prevent gut and brain dysfunctions in SAMP8 mice. Our results show that butyrate alleviates amyloid pathology, neuroinflammation and prevents gut dysmotility and memory loss in AD model.

MATERIALS AND METHODS

Ethics statement

All experimental procedures involving animals were approved by the Ethics Committee of Nantes University and Inserm for Animal Use in Research, and all methods were performed in accordance with the relevant guidelines and regulations.

Animals

SAMP8 mice and control littermates were bred in-house and were previously described [21]. Animals were housed on a reverse light–dark cycle. Care and experimental manipulation of animals were in accordance with French standard ethical guidelines for laboratory animals. For each time course experiment, two cohorts of animals were used, with littermates randomized to the appropriate groups before manipulation. Mice were randomly assigned to experimental groups and all the experiments were performed double-blinded. Animals were used according to "3Rs" principles (Replacement, Reduction and Refinement) in all experimental procedures. Mice were euthanized at the indicated time points to collect tissue for analyses and comparison. Data collection and analyses were performed blinded to the conditions of the experiments and subsequently reported to genotype and/or treatment. Tg2576 mice [22] tissues were provided by Université Toulouse III - Paul Sabatier Centre de Biologie Intégrative Centre de Recherches sur la Cognition Animale - CNRS UMR 5169. Sample sizes were determined based on previous animal studies to ensure adequate power to detect significant differences ($p < 0.05$).

Oral butyrate supplementation

In a previous study, 8 g/liter of butyrate was administered via drinking water for 8 weeks to modulate neuroinflammation in mice [23]. Here, we used half of that concentration because butyrate was chronically administered to mice in drinking water for a longer period of time. Briefly, 4 groups of mice were set-up at weaning (3-week-old, n = 10–15 mice per group). Sodium butyrate was given for 5 months in drinking water (*ad libidum*) at a concentration of 4.4 g/liter (control groups received water only). After 5 months of continuous butyrate supplementation, mice were tested in vivo for gut functions, then subjected to behavior tests. After euthanasia, blood and tissues from colon and hippocampus were collected for ex vivo analysis. Body weight was recorded 3 days a week.

Tissue dissection and immunohistochemistry procedures

Gut histology—Segments of mouse proximal colon were fixed in 1X PBS containing 4% paraformaldehyde for 3 h at room temperature or at 4 °C overnight. Whole mounts of longitudinal muscle and myenteric plexus were obtained by microdissection and were first permeabilized with PBS-NaN3 1% sodium azide containing 4% horse serum and 0.5% Triton X-100. Tissues were then incubated with primary antibodies (Supplementary Table 1) overnight. After several washes in PBS, tissues were incubated for 1 h at room temperature with the appropriate FITC-conjugated or Alexa 568-conjugated secondary antibodies diluted in PBS-NaN3 4% horse serum 0.5%Triton X100. Tissues were washed with PBS and mounted with ProLong Gold Antifade Reagents with DAPI (Molecular Probes, Carlsbad, CA, USA).

Brain histology—Brain left hemisphere were extracted from mice and post-fixed in 4% PFA in PBS for 16–20 h at 4 °C then transferred to a 30% sucrose solution in 1X PBS until saturation. Serial coronal sections 35-µm thick were cut using a cryostat (Microm HM 560 MV) and preserved in a cryoprotectant (25% glycerol /25% ethylen glycol /50% 0.2 M PBS) at -20 °C until use. Coronal sections were rinsed three times with 1X PBS. Floating sections were blocked with 3.5% Hose Serum and 0.5% 100X Triton in 1X PBS for 2 h at room temperature and incubated in primary antibody (Supplementary Table 1) in the same buffer overnight at 4 °C on a shaker. Sections were washed three times with PBS and then incubated with appropriate secondary antibodies diluted in PBS with 3.5% Hose Serum/ 0.5% 100X Triton in 1X PBS. Sections were washed three times in PBS, mounted with ProLong Gold Antifade Reagents (Thermo Fisher, P36930) on coverslips for confocal imaging.

Primary cultures

ENS culture—Primary cultures of rat enteric nervous system (ENS) were performed as previously described [24]. Briefly, embryonic day 15 (E15) rat intestine were removed and finely diced in Hank's buffered salt solution and triturated mechanically using a scalpel. Tissue fragments were collected in Dulbecco's modified Eagle medium (DMEM)/F12 (1:1) medium (Life Technologies, Carlsbad, CA, USA) containing 50 µg ml^{-1} streptomycin and 50 U ml^{-1} penicillin and incubated for 15 min at 37 °C in the same medium containing 0.25% trypsin (Invitrogen). After 15 min, the reaction was inactivated by adding 10% fetal bovine serum (FBS) for 5 min. Samples were incubated for 10 min at 37 °C with 0.1% DNase I (Sigma, St Louis, MO, USA). After trituration and centrifugation for 10 min at 84 g, cells were plated in DMEM (Thermofisher #1966025) /F12 (Thermofisher #11765054) containing antibiotics and 10% 1X FBS at a density of 2.4×105 cells cm^2 on 24-well plates previously coated with 0.5% gelatin (Sigma) for 24 h. Medium was replaced with fresh DMEM/ F12 without serum and supplemented with 1% N2 (Invitrogen #17502048). Half of the medium was replaced every 3 days, and primary cultures were maintained for up to 14 days.

Pure enteric neuron culture—Isolation and dissection of rat intestines have been previously described [25]. Briefly, embryonic day 15 (E15) rat intestines were collected and dissected in cold Hank's buffered salt solution (HBSS). Each whole intestine (duodenum to sigmoid colon) was individually placed in a drop of cold HBSS in a Petri dish and cut into 8 pieces of equal length. Pieces were placed in a 24-well plastic culture plate (Corning®-115 Costar®, ref 3524, Merck KGaA, Darmstadt, Germany) previously coated with type I collagen/20 mM acetic acid and containing an enteric glial cell (EGC)-conditioned culture medium with 50 ng/mL GDNF (R&D Systems–bio-

techne, 512-GF-050/CF). EGC cultures were obtained from enteric nervous system (ENS) primary cultures derived from rat embryonic intestines [26]. EGC-conditioned medium was filtered through a sterile 0.22 µM Poly-EhterSulfone membrane before storage at -20 °C until use. After 5 days of culture (D5), many cells migrated from the explants and covered a large part of the well. Explants were removed using a P1000 pipette, and cells were isolated with 300 µL of Accutase per well for 5 min. Accutase was inactivated by adding 4.7 mL of DMEM + FBS and cell suspensions were centrifuged at 1500 rpm for 5 min at room temperature. Cell pellets were suspended in EGC-conditioned medium + GDNF (50 ng/mL) and seeded in previously poly-L-lysine (0.1 mg/mL)-coated P24 plate for immunofluorescence, on 18 mm diameter coverslip (Neuvitro corp., Vancouver, WA, USA) for patch-clamp, Ibidi 8-well plate for Ca^{2+} and imaging. At D6, an antimitotic (cytosine arabinoside: AraC, 5 µM) was added to the medium to eliminate the remaining glial and muscle cells. Purified neurons were used for functional and morphological tests at DIV11 and DIV12.

Homogenization and immunoblotting

Tissues— Brain or colon tissues were placed in 1X RIPA buffer (Millipore) diluted in distilled water with a protease inhibitor cocktail (Thermo Fisher, A32963) and homogenized in 2 ml bead tubes (Macherey-Nagel) using a Precellys 24 (Bertin Technologies). Homogenates were centrifuged and protein concentration was determined in supernatant using a BCA assay (Thermo Fisher).

ENS and pure enteric neuron cultures— Cultures were scrapped into 1X RIPA buffer containing protease cocktail inhibitor, pelleted by centrifugation and protein concentration was determined in supernatant using a BCA assay (Thermo Fisher).

Immunoblotting—For western blotting, 35-50 µg of protein from fresh or previously frozen lysate was separated by 4–12% Bis-Tris gels (Thermo Fisher, WBT4122) with MES SDS NuPAGE running buffer (Thermo Fisher, NP0002) and transferred to nitrocellulose membranes (25 V, 7 min) (Thermo Fisher, IB23001) with the iBlot2™ Dry Blotting System (Life Technologies). On orbital shakers, membranes were blocked with non-fat dry milk in Tris-buffered saline with 0.1% Tween-20 (TBS-T) for 2 h at room temperature and then incubated with primary antibodies (Supplementary Table 2) in TBS-T at 4 °C overnight. Membranes were washed three times in TBS-T and incubated with fluorescent or horseradish peroxidase (HRP)-conjugated secondary antibodies in TBS-T for 2 h at room temperature on an orbital shaker. Membranes were again rinsed three times in TBS-T. A Bio-Rad ChemiDoc MP was used to detect fluorescence or HRP-conjugated secondary antibodies by using Pierce ECL (Life Technologies, #32209), Supersignal™ West Pico (Life Technologies, #34580) or Supersignal™ West Femto (Life Technologies, #34096) substrate). Densitometry analysis was performed using ImageJ or Image-Lab (Bio-Rad).

Real-time RT- qPCR

RNA from gut and brain tissues of mouse was isolated using the Nucleo Spin RNA Triprep Kit, according to the manufacturer's instructions. Potential genomic DNA contamination was removed by treatment with Turbo™ DNase (Ambion Inc., Austin, TX, USA) and RNA was quantified using an ND-1000 UV-Vis spectrophotometer (Nanodrop Technologies, Wilmington, DE, USA). cDNA was synthesized from 1 µg total RNA using the Super Script III Reverse Transcriptase System kit (Invitrogen) and diluted to a final concentration of 8 ng eq RNA/µL. qPCR was performed using StepOne Plus (Life Technologies) detection system with Fast SYBR Green (Life Technologies) master mix. The PCR signal was normalized against S6 as reference gene to control for variability in the amount and quality of the RNA. The sense and antisense oligonucleotide primers used in this study are shown in supporting information (Supplementary Table 3**)**.

Aβ preparation

Recombinant human Aβ1-42 peptides (AG968-1MG Sigma-Aldrich) were lyophilized in hexafluoroisopropanol (HFIP), reconstituted in dry dimethyl sulfoxide (DMSO) at 2.2 M, diluted in DMEM medium (pH 7.4) (Invitrogen, Carlsbad, CA) to 1 µg /µl, incubated at 4 °C for 48 h, and stored at −80 °C until use. For treatment of cells, stock solutions of Aβ peptides were diluted in fresh culture medium to final concentrations of 1 µg/ml. This type of preparation contained Aβ oligomers but no fibrils [27].

Colonic intramuscular injections

Mice were anesthetized with 1–4% isoflurane and placed in a supine position on a self-regulating heating pad. The hair over the abdomen was removed and a 2-cm incision was made along the midline. The colon intestinal lining was directly injected at three sites, 0.5 cm apart, below and above the cecum with a 10 µl Hamilton syringe equipped with a 36-gauge beveled needle (World Precision Instruments). Each site was injected with 3 µl of saline containing 1 µg/µl of Aβ preparation or 3 µl saline alone. After injection, the colon was carefully replaced and the skin was sutured. Mice were euthanized 1-month post-injection and underwent gut functional and biochemistry analysis.

Cultures treatment

Sodium butyrate was obtained from Sigma Aldrich (reference#B5887). For rescue experiments with exogenous Aβ, 5 DIV ENS cultures or pure enteric neuron cultures were pre-treated with indicated concentrations of sodium butyrate for 12 h and then 1uM Aβ was added for 24 h. Control neurons were treated only with the vehicle solution (PBS). For rescue experiments with SAMP8 enteric neurons, butyrate was chronically added directly to 10 DIV cultures, each day for 4 consecutive days. Dose-response on WT enteric neurons was conducted by adding different concentrations of butyrate to 13 DIV ENS or pure enteric neuron cultures for 24 h. Time-course experiments on enteric neurons or ENS cultures were conducted by adding 1µM Aβ for indicated time points.

Immunostaining on cell cultures

Cells were fixed in PBS containing 4% paraformaldehyde for 15 min. Cells were permeabilized for 5 min at room temperature in 0.25% Triton-X-100 in PBS, washed twice with PBS, and incubated for 30 min at 37 °C in PBS containing 10% BSA. Neurons were incubated overnight at 4 °C with primary antibodies diluted in PBS containing 3% BSA and 0.02% azide. Antibodies used are listed in Supplementary Table 1. After washing, cells were incubated for 90 min at room temperature with the appropriate FITC-conjugated or Alexa 568-conjugated secondary antibodies diluted in PBS containing 3% BSA and 0.02% azide. Cells were washed with PBS and mounted with ProLong Gold Antifade Reagent with DAPI (Molecular Probes).

LDH assay

Lactate Dehydrogenase (LDH) assay Kit was purchased from Abcam (reference #ab102526) and used per manufacturer recommendations. Briefly, cell lysates were diluted in assay buffer based on preliminary experiments to make sure the readings are within the range of the standard curve and samples and LDH Positive Control were kept on ice during the assay. Five µl of LDH positive control or samples were added in duplicates to 96-well plate containing 45 µl of assay Buffer and 50 µl of the Reaction Mix was added to each well (Standards, Positive Control and samples). The OD450 is red immediately (A1). The plate was incubated at 37 °C for 20 min (or longer if the LDH activity is low) and OD450 was measured again as A2. Data were analyzed by subtracting the 0 nmol/well NADH background from Standard readings and plot NADH Standard Curve. LDH is calculated based on formula: LDH Activity = [B x Sample Dilution] ÷ [incubation time x V]. V is the volume of diluted sample into the reaction well in ml.

ELISA quantification of Aβ

Colon and hippocampal tissues from SAMP8 mice and control littermates were homogenized in 2% sodium dodecyl sulfate (SDS) with protease inhibitors. Then, the homogenates were centrifuged at 4 °C for 1 h at 100,000 g. The supernatant containing soluble Aβ was then aspirated into a tube. Quantitative determination of Aβ was then performed using solid phase sandwich enzyme-linked immunosorbent assay (ELISA) kits for the determination of $Aβ_{1-40}$ and $Aβ_{1-42}$, in accordance with the manufacturer's instructions (Thermo Fisher Scientific). In brief, 50 µL standards of Aβ (to create a gradient of concentrations) and protein samples were added to an Aβ antibody-bedded plate, and then 50 µL of detection antibody was added. After incubation for 1 h at 37 °C, the liquid was discarded and the wells were washed four times for at least 30 seconds. Then, 100 µL of anti-rabbit horse radish peroxidase (HRP) working solution was added to the wells and incubated for 30 min at room temperature followed by 100 µL of stabilized chromogen for 30 min at room temperature in the dark. Then, we added 100 µL of stop solution and the absorbance of each well was read at a wavelength of 450 nm using a Synergy H1 plate reader (Biotek, Agilent). The concentrations of $Aβ_{1-40}$ and $Aβ_{1-42}$ were calculated by standard curve fitting.

BACE1 enzymatic assay

BACE 1 activity assay Kit was purchased from Abcam (reference #ab282921) and used per manufacturer recommendations. Briefly, 50 µl of cell lysates supernatant were diluted in assay buffer (48 µl assay buffer and 2 µl of BACE1 substrate) for 100 µl total. The 96-well plate containing samples and reaction Mix (Standards, Positive Control) is red immediately in kinetic mode for 30-60 min at Ex/Em= 345/500 nm at 37 °C. The 0 standard reading is subtracted from all readings. BACE1 activity is calculated based on formula: Sample BACE1 Activity = B/(Δt X V) x D = pmol/min/µl = µU/µl = mU/ml.

Imaging and immunoblot quantification

IHC—To determine the number of neurons and interganglionic connections, images were acquired with a ×20 objective using a digital camera (DP50, Olympus) coupled to a fluorescence microscope (BX51, Olympus). The camera was driven by Olympus DP-Soft version 3.2. Each cell type was scored and normalized to the total number of Hu-positive cells. For each experiment, a least 5 independent mice were counted per group. The number of neurons per field (Hu-positive cells) was counted on eight fields of view from a ×20 objective for each experiment. To determine the number of ganglia, defined by at least two aggregated neurons, half of the surface coverslip was scanned with a ×10 objective and the number of ganglia was scored. The number of neurons per ganglion were scored on at least 10 ganglia per condition.

Immunoblots—Analyses of western blots was performed in ImageJ or Image Lab (Bio-Rad). Regions of interest (ROIs) were drawn around bands of interest or the length of the lane (for S129P) and the integrated density was measured. Relative integrated densities were calculated against the average of the WT samples on each membrane and normalized to housekeeping genes (β-actin or β-tubulin) or total protein (Stain Free Gels, Bio-Rad).

Analyses of immunohistochemical signals was performed in ImageJ. ROIs were drawn as delineated by the presence of the neurotransmitter signal specific to the region (for example, ChAT or Tuj1 for the myenteric plexus) and the integrated density was measured. Integrated densities were calculated per unit area and normalized to the average from WT samples.

Calcium imaging— Analyses of calcium signals was performed in ImageJ. Acquired video signals were loaded as image stacks and ROIs were drawn around each cell exhibiting jRGECO1a signal. An integrated density measurement was taken of the entire image stack for each cell. The percentage change in fluorescence after the photostimulation pulse was calculated by dividing the integrated density signal by the average of the 20 frames (2 s) that preceded the blue light pulse. Data were analyzed in GraphPad Prism to determine the area under the curve.

Thioflavin S staining

Brain coronal sections were rinsed 30 min by using distilled water followed by three five-minute washes with 0.1 M PBS, then sections were incubated in 0.01% Thioflavin S (ThioS) in 50% ethanol for 8 min before being washed three times with 50% ethanol for 5 min per wash and mounted with ProLong Gold Antifade Reagents (Thermo Fisher, P36930) on coverslips for confocal imaging. ThioS images were captured with a confocal fluorescence microscopy (Nikon).

Calcium imaging

Ca^{2+} imaging was performed by using Cal-520, AM dye (Abcam, Cambridge, UK) in Ibidi 8-well plates (µ-Slide 8 Well, #80826, Gräfelfing, Germany) as previously described [25]. Briefly, 10DIV pure enteric neurons were treated 24 h with Aβ (1 µg/ml) or sham and loaded into glia-conditioned medium supplemented with Cal-520 AM dye (5 µM) for 60 min at 37 °C in a cell culture incubator. High-frame-rate (60 fps) images were recorded using a resonant scanning NIKON A1 RSi confocal microscope (Nikon Instruments, Champigny sur Marne, France) with a dedicated oil immersion objective (×63, NA, 1.40) and a temperature (37 °C)/CO2 (5%) controller. The dye was excited by a laser source at 488 nm and the fluorescence signal was recorded at 520 nm. Images were analyzed with the ImageJ software. The fluorescence intensity was measured in region of interest (ROI) delimitating neuronal cell bodies for spontaneous activity and upon pharmacological stimulations. Data were represented as changes in fluorescence intensity according to the formula $\Delta F = F/F0$, where F0 is the minimum fluorescence intensity. Analyses were carried out on a total of 3x field per well with at least 30 neurons per field from at least 3-6 wells per condition and 3 independent cultures. Cells were stimulated with 30 µM veratridine (Sigma). Signal analysis was carried out on a total of 360 neurons from n = 4-6 culture wells per condition.

Electrophysiology

Patch-clamp—Enteric mixed cultures (ENS) cells were grown for 10 days on glass coverslips and incubated with Aβ (1 µg/ml) or sham for 24 h. Glass coverslips were then transferred into a recording chamber and continuously perfused with Ringer's saline buffer containing 140 mM NaCl, 4 mM KCl, 2.5 mM CaCl2, 1 mM MgCl2, 10 mM HEPES, 11 mM glucose, buffered to pH 7.4, at 22-24 °C (room temperature). Recording pipettes (5–7 MΩ resistance) were filled with 135 mM CsCL, 0.3 mM EGTA, 10 mM HEPES, 4 mM MgATP, 0.3 mM NaGTP and titrated to pH 7.2 with CsOH. Cells were continuously perfused with extracellular solution, at a rate of 2 ml/min. SNE cultures were visualized under an Olympus BX51WI microscope (Olympus, Rungis, France), with a 4x/0.13 objective for the placement of the stimulating electrode and a 40X/ 0.80 water-immersion objective for the localization of cells for whole-cell recordings. Voltage-clamp recordings were filtered at 5 kHz and sampled at 10 kHz, with the Patchmaster program (HEKA Elektronik). The series resistance was compensated at 75–80%. Spontaneous currents were measured using a Cs-high-chloride based intracellular solution. Neurons within ganglia were voltage clamped at -60mV and the current were analyzed during 250 s recording segments. The spontaneous post-synaptic currents (sPSCs) were identified by using a semi-automated amplitude threshold-based detection software (Mini Analysis 6.0.7 Program, Synaptosoft, Fort Lee, NJ, USA).

Behavior

All behavior tests were recorded using an automated infrared photobeams detection system (Videotrack v2.6) and an analysis software (ViewPoint).

Novel object recognition—Mice were transferred to the testing room and acclimated for at least 1 h before testing. The testing was performed in a white round plastic chamber (43 ×43 x 30 cm). On day 1, mice were habituated to the testing arena for 30 min. On day 2, each mouse was presented with two identical objects in the same chamber and allowed to explore freely for 10 min. Three hours after this training session, mice were placed back into the same arena for the test session, during which they were presented with an exact replica of one of the objects used during training and with a novel, unfamiliar object of different shape and texture. Object locations were kept constant during training and test sessions for any given mouse, but objects were changed semi-randomly between mice. Arenas and objects were cleaned with Surfa'safe (Anios) after each recording. Behavior was recorded with a video tracking system (Viewpoint). Frequency of object interactions and time spent exploring each object were recorded for subsequent data analysis. As precondition, animals that freeze during training sessions in the NOR bevavior test are excluded.

Y-Maze—Working memory was assessed using the Y-maze test. There were three identical arms of 30 × 10 × 20 cm and a triangle connecting the center area to the 10 × 10 × 10 cm arms. Each arm formed a 120° angle with the other two arms. The mice were placed at the end of one arm and allowed to move freely through the maze for 5 min. A record was kept of the order in which the mice chose to enter the arms. An alternation of three consecutive choices with different arms was scored as one point. Taking the total number of arm entries minus two, the total number of opportunities for alternation was calculated. The % correct rate = (total alternation points/total alternation opportunities) × 100. Between trials, Surfa'safe (Anios) was used to clean up the Y-maze. As precondition, animals that freeze during testing sessions in the Y-Maze bevavior test are excluded.

Elevated plus-maze—The elevated plus maze consisted of two open (without walls) and two enclosed (with walls) arms elevated 63 cm above the ground (Viewpoint Behavior Analysis Technologies, Lyon, France). Mice were allowed to habituate in the testing room under dim light for 1 h before testing. During testing, mice were placed at the junction between the open and closed arms of the plus maze and allowed to explore for 5 min. The maze was cleaned with Surfa'safe (Anios) between testings. Total distance traveled and time spent in both the open and closed arms were calculated for data analysis.

Open field—Before testing, mice were transferred to the testing room and acclimated for at least 1-h. Mice were tested in square plastic chambers (43 ×43 x 30 cm) for 15 min, with with infrared camera recording ambulatory movements. The apparatus was cleaned with Surfa'safe (Anios) between testing. Total movements in the outer periphery and center of the open field were recorded for further data analysis.

Gut functional exploration

To assess fecal pellet output (FPO), mice were placed individually in a clean cage without bedding, food and water for fecal pellet collection. Fecal pellets were monitored at 5 min intervals for the presence of carmine red. Fecal pellets were collected and counted every 15 min for 2 h. Total transit time was defined as the interval between the initiation of gavage and the time of first observance of carmine red in feces.

Human iPSC-derived intestinal organoids

Human intestinal organoids containing an enteric nervous system (HIO + ENS) were generated as previously described [28]. Briefly, human induced pluripotent stem cells (iPSCs) were fed with mTeSR1 media and routinely passaged using XF passaging solution (Miltenyi Biotec). Neural crest cells (NCCs) and HIOs were generated and combined them at an early stage of intestinal differentiation to generate HIOs+ENS. Briefly, for NCC generation, human iPSCs were treated with collagenase IV (500 U/ml) in mTeSR1 for 60 min to detach colonies. Cells were washed to remove collagenase, then gently triturated and resuspended in neural induction media. Neural induction media was changed daily, and retinoic acid (RA, 2 µM) was added on days 4 and 5 for posteriorization. Day-6 free-floating neurospheres were plated on fibronectin (3 µg/cm2) and fed neural induction media without RA for 4 d. Migrated cells were collected using a brief Accutase treatment (2-3 min) and passaged onto fibronectin or used immediately for combining with HIOs. NCCs were differentiated and HIOs were generated by using cytokine Activine A, growth factor FGF4 and small molecule CHIR99021. After the formation of gut tube spheroids, NCCs and spheroids were centrifuged for 2 min at 300 g with a ratio of 600-1000 NCCs per spheroid and embedded in Matrigel drops. Cultures were fed a basic gut media (advanced DMEM/F12, 1× B27 supplement, 1× N2 supplement, 10 µM HEPES, 2 mM l-glutamine, 1× Pen-Strep) supplemented with 100 ng EGF ml−1 and maintained in vitro for up to 28 DIV.

Explant cultures of human colon

Colon specimens were cultured as previously described [29]. Briefly, colons were obtained from 3 distinct patients undergoing surgery for colon carcinoma. Fragments of the human proximal colon were taken at about 10 cm downstream to the tumor. Tissue fragments were processed according to the French guidelines for research on human tissues. Informed patient consent was obtained, according to the French bioethics law. Immediately after removal, tissues were placed in 4 °C oxygenated Krebs solution, and the mucosa was carefully stripped from the underlying compartment made of muscularis mucosae and submucosa. Fragments of 20–30 mg were cut out and pinned in Sylgard-coated Petri dishes and maintained in culture for 24 or 48 h in 2 ml 500 ml DMEM / HAM F12 (Invitrogen 31330-038) with 1.05 NaHCO3 containing Nifedipine (1uM). Then 5 ml of antibiotics (Sigma A7292), 1 ml of Gentamicin (Sigma G1272) 0.125 ml of Amphotericin B (Stock solution 10 mg/ml Sigma A9528), and 50 ml of callfserum was added to the culture media. The explants were maintained at 37 °C in a 95% oxygen, 5% carbon dioxide humid atmosphere on a shaker platform at low speed.

Statistics

Cells were processed and randomly divided between vehicle controls and treated groups for in vitro experiments. All in vitro experiments were obtained from at least 3 independent ENS or pure enteric neuronal cultures with 6 wells per condition each culture. Animals were sex mixed and randomly assigned to treatment and control groups. Investigators were blind to group allocation during data collection and analysis. Means of two groups were compared using unpaired Student's *t*-tests or Mann-Whitney. Normally distributed continuous variables were compared using one- and two-way ANOVA with Tukey's multiple comparisons test. Non-normally distributed data were analyzed using nonparametric Kruskal–Wallis test followed by Dunn's multiple comparisons test. Microsoft Excel v. 16.89.1 (24091630) was used to collect data. The statistical software package used is Prism 10 (GraphPad Software). All data are presented as mean ± SEM unless otherwise noted.

RESULTS

Early ENS dysconnectivity, GI deficits and Aβ accumulation in SAMP8 mice

To explore gut function, we used SAMP8 mice, which are widely used for studying age-related amyloid pathology, cognitive deficits, neuroinflammation and evolution towards a sporadic AD [21]. We found that fecal pellet output (FPO) was lower and gut transit time was higher in 2-month-old (2mo) and 6-month-old (6mo) SAMP8 mice as compared to controls (Fig. 1a,b). Intestinal length was similar between groups (Supplementary Fig. 1a), ruling out a potential effect on gut transit and FPO. Moreover, SAMP8 mice displayed a lower body weight relative to controls in both age groups (Supplementary Fig. 1b).

Next, we examined AD-related behavior in the novel object recognition (NOR), elevated-plus maze (EPM) and open field (OF) tasks, which measure short- or long-term recognition memory, anxiety-like behavior and ambulatory locomotor activity, respectively. The NOR test revealed a memory deficit in 6mo, but not 2mo, SAMP8 mice relative to controls (Fig. 1c). Furthermore, 2mo and 6mo SAMP8 showed emotional disorders, such as reduced anxiety-like behavior or disinhibition, relative to age-matched littermates as shown by an increased time spent in the open arms during the EPM test (Fig. 1d). Ambulatory locomotor activity was increased in 6mo, but not 2mo, SAMP8 mice in OF test (Fig. 1e). Altogether, these data indicate that gut symptoms occur prior to memory decline and ambulatory locomotor hyperactivity, but not disinhibition, in SAMP8 mice.

We have previously shown that EphB2 tyrosine kinase and synaptophysin regulate the connectivity and activity of gut and brain neurons [15, 16]. To examine whether ENS connectivity is altered in SAMP8 mice, we first measured expression levels of EphB2 and synaptophysin in whole colon lysates. EphB2 was significantly decreased in 2mo and 6mo SAMP8 mice, whereas synaptophysin was decreased in 6mo, but not 2mo, SAMP8 mice relative to controls (Fig. 1f). We next examined the ENS network structure in the colon myenteric plexus. We carried out immunofluorescent colocalization studies of HuC/D, broad neuronal markers in the ENS, Tuj1 and Aβ, which revealed a decrease of Tuj1-immunoreactive (Tuj1-IR) interganglionic fibers within the myenteric plexus, suggesting a decrease of enteric neuronal connectivity, and an increase of Aβ on neuronal soma and along interganglionic fiber tracts (Supplementary Fig. 1e–h). However, we observed no difference in overall neuronal density, in 2mo and 6mo SAMP8 mice relative to controls as shown by the equal number of HuC/D-IR neurons between groups. In addition, we measured the expression of key enzymes such as choline acetyl transferase (ChAT) and neuronal nitric oxide synthase (nNOS), which are respectively involved in the synthesis of ACh and NO, two crucial neuromodulators of gut motility [30]. Interestingly, in 2mo SAMP8 mice, the number of nNOS-positive (nNOS +), but not ChAT-positive (ChAT +), neurons were significantly decreased and the total number of HuC/D-IR neurons remained unchanged (Supplementary Fig. 2a,b). However, in 6mo SAMP8 mice, both ChAT+ and nNOS+ neurons were significantly decreased with no change in overall HuC/D-IR neurons (Supplementary Fig. 2c,d). To determine whether above mentioned alterations occur in another AD model, we examined the TG2576 transgenic mice over-expressing APP with the Swedish mutation [22]. Similarly to SAMP8 mice, we observed a decreased expression of ChAT and nNOS (Supplementary Fig. 2e,f) as well as a depletion of EphB2 and synaptophysin (Supplementary Fig. 2g) in the colon of TG2576 mice as compared with NTG mice, suggesting that ENS lesions are not specific to SAMP8 mice, but rather a pathologic feature that extends to AD transgenic models.

AD is characterized by abnormal secretion/production of Aβ and its accumulation in the brain, causing detrimental effects to neurons in the central nervous system (CNS). Our data and previous reports in other pre-clinical models and in patients have shown exacerbated Aβ levels in the gut [31]. However, the cell-type that produce in the gut remains elusive. To explore whether the ENS network produces Aβ, particularly neurons, we cultured primary enteric neurons isolated from SAMP8 mice via a method we previously developed [25]. We carried out immunofluorescent

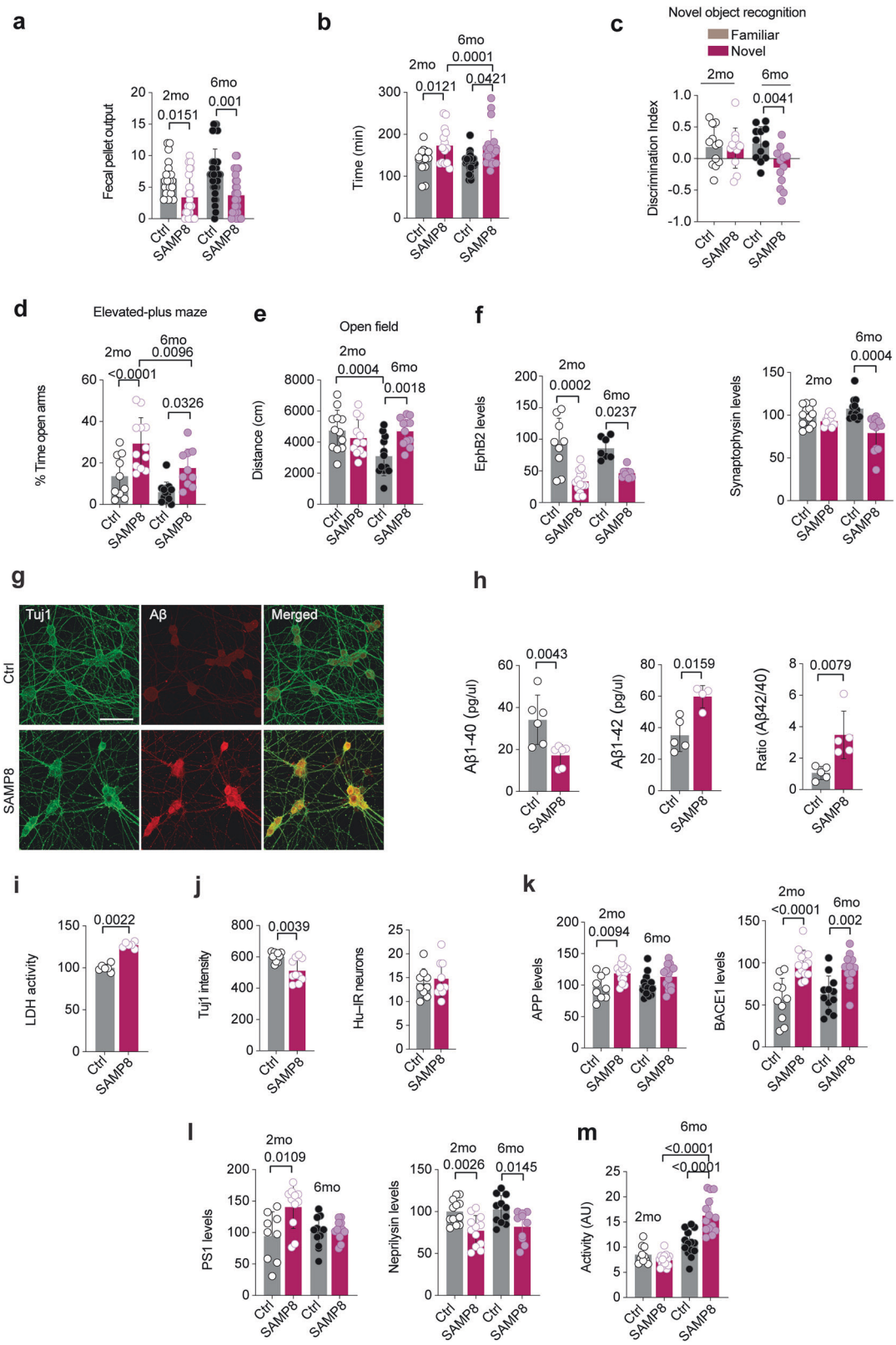

(IF) staining to visualize and confirm Aβ production and binding to neuronal cells. Although Aβ was detected at low levels in control cultures, it was present at significantly higher levels at the soma and in punctiform clusters along neuronal processes of enteric neurons isolated from SAMP8 mice (Fig. 1g). To confirm an increase of Aβ production by SAMP8-derived enteric neurons, we measured concentrations of its soluble forms $A\beta_{1-40}$ and $A\beta_{1-42}$ in culture media collected after 14DIV. Enzyme-linked immunosorbent assay (ELISA) showed lower $A\beta_{1-40}$ levels, but increased $A\beta_{1-42}$ concentration and ratio of $A\beta_{1-42}$/ $A\beta_{1-40}$ in media collected from SAMP8-derived neurons relative to Ctrl condition (Fig. 1h).

Fig. 1 SAMP8 mice develop an early amyloid pathology and gut impairments. a FPO measure for 2 h in 2mo and 6mo Ctrl and SAMP8 mice. Two-way ANOVA and Tukey's multiple comparisons (*n* = 21-34 animals per group). **b** Gut transit time measured in mice from **a**. Two-way ANOVA and Tukey's multiple comparisons (n = 14-32 animals per group). (**c-e**), NOR (**c**), EPM (**d**) and OF (**e**) of 2mo and 6mo Ctrl and SAMP8 mice. NOR, discrimination index differences were assessed with paired t-tests. Discrimination index of 0.5 indicates chance preference (*n* = 11–15 mice per condition); EPM and OF, Two-way ANOVA and Tukey's multiple comparisons, (n = 11-15 animals per group). **f** Quantification of EphB2 and synaptophysin proteins in the colon of 2mo and 6mo Ctrl and SAMP8 mice. Mann-Whitney test (n = 8-12 animals per group). **g** IF staining of Tuj1 (green) and Aβ (red) in pure enteric neurons cultured from Ctrl and SAMP8 mice. Scale bar, 20 µm. **h** ELISA quantification of Aβ levels in culture media conditioned from14 DIV pure enteric neurons isolated from Ctrl and SAMP8 mice. Mann-Whitney (n = 4–6 animals per group). **i** LDH measures in conditioned culture media obtained from pure enteric neurons cultured from Ctrl and SAMP8 mice. Mann-Whitney (n = 9–10 animals per group). **j** Quantification of Tuj1 and HuC/D IF signals in pure enteric neurons isolated from Ctrl and SAMP8 mice. Mann-Whitney (n = 8–10 animals per group). **k**, **l** Quantification of APP, BACE1, PS1 and neprilysin proteins in the colon of 2mo and 6mo Ctrl and SAMP8 mice. Mann-Whitney (n = 9–14 animals per group). **m** Measure of BACE1 activity in colon whole lysates of 2mo and 6mo Ctrl and SAMP8 mice. Two-way ANOVA and Tukey's multiple comparisons (n = 10–14 animals per group).

This was associated to an increase in lactate dehydrogenase (LDH) release in culture media by SAMP8 neurons, which assess the level of plasma membrane damage in a cell population (Fig. 1i), and a decrease of Tuj1 signal intensity without an overall significant change in enteric neuron density, as assessed by neuronal count of HuC/D-immunoreactive (IR) cells (Fig. 1j). Increased Aβ production could result from an exacerbated APP processing by β-secretase BACE1 [32] and γ-secretase, which comprises presenilin-1 (PS1) [33] or a deficient clearance by enzymes degrading Aβ such as the endopeptidase neprilysin [34]. We found that APP, BACE1, PS1 protein expression were increased, whereas neprilysin was decreased in the colon of 2mo SAMP8 mice and some of these changes were sustained in 6mo SAMP8 (Fig. 1k,l and Supplementary Fig. 2h). Although BACE1 activity was not different between groups in 2mo mice, it was significantly increased in 6mo SAMP8 relative to controls (Fig. 1m). Taken together, these data suggest that an early increase in APP holoprotein coupled with higher levels of enzymes involved in its amyloidogenic processing are associated to Aβ accumulation in the ENS of AD mice.

Aβ impairs enteric neuronal connectivity and activity in vitro

To determine whether Aβ alters ENS connectivity, we exposed pure enteric neuron cultures to exogenous preparation of Aβ, which contains different species of oligomeric $Aβ_{1-42}$ and monomers (Fig. 2a) [35]. Analysis of immunofluorescence imaging after Aβ exposure revealed its colocalization within neuronal processes and soma in puncta-like structures that are reminiscent of endogenous Aβ profile in SAMP8 enteric neurons (Fig. 2b). In non-treated neurons, endogenous Aβ was present at lower levels and mainly confined at the neuronal soma. LDH release was increased in Aβ-treated enteric neurons as compared to control condition (Fig. 2c). Furthermore, we examined effects of exogenous Aβ on WT enteric neurons. IF imaging revealed lower levels of Tuj1-immunoreactive (IR) neuronal processes in Aβ-treated enteric neurons and no difference in number of Hu-IR neurons relative to control condition (Fig. 2d and Supplementary Fig. 3a). We also found that Aβ significantly reduced EphB2 and synaptophysin (Fig. 2e,f) in a dose- (Supplementary Fig. 3b,c) and time-dependent (Supplementary Fig. 3d–f) manner. These data suggest that Aβ causes a neurotoxicity and impairs interganglionic fiber tracts.

We have previously shown that EphB2 and synaptophysin are master regulators of neuronal plasticity and function [15, 16]. To examine the impact of Aβ-induced depletion of these synaptic proteins on enteric neurons, we measured spontaneous miniatures of post-synaptic currents (mPSC) by patch-clamp recordings in ENS cultures after 24 h exposure to Aβ (Fig. 2g). We found that mPSC amplitude and frequency (Fig. 2h), but not rise time and decay time (Supplementary Fig. 3g), were significantly decreased in primary culture of ENS following Aβ treatment. Using a Ca^{2+} imaging approach, we assessed the Aβ capacity to modulate spontaneous neuronal activity by measuring Ca^{2+} transients in pure enteric neurons [25]. Enteric neurons exposed to Aβ exhibited spontaneous activity in the cell body (Fig. 2i) with a decrease of Ca^{2+} transients mean amplitude, AUC and frequency relative to vehicle-treated neurons (Fig. 2j). Similarly, these parameters were impaired in pure enteric neurons isolated from SAMP8 mice (Fig. 2k,l). We further examined Aβ effects on neuronal activity by measure of veratridine-evoked-Ca^{2+} signals, a voltage dependent Na^+ channel opening agent that causes Ca^{2+} influx [36]. Veratridine-evoked Ca^{2+} transient was impaired in enteric neurons exposed to Aβ relative to control (Ctrl) condition (Supplementary Fig. 4a,b). Similarly, measures conducted in neurons cultured from SAMP8 mice revealed an impairment of veratridine-evoked Ca^{2+} transient relative to Ctrl neurons (Supplementary Fig. 4c,d). Together, these data suggest that Aβ impairs enteric neuronal connectivity and activity in vitro.

Aβ disrupts ENS connectivity in mice and in human in vitro models

Previous studies have shown the presence of Aβ aggregates in the gut of AD pre-clinical models [37, 38] and that soluble oligomers of Aβ can bind to different components of neuronal and non-neuronal plasma membranes in the CNS to induce synaptic dysfunction underlying memory loss in AD [13]. However, it is unclear whether Aβ can directly alter ENS connectivity and GI function in vivo. To examine this possibility, we reproduced a gut amyloid pathology by seeding the colon of 3mo wild-type (WT) mice with exogenous Aβ preparation through a direct intracolonic injection of Aβ (Fig. 3a). One month after surgery, Aβ-injected mice displayed a reduced FPO relative to control group (Fig. 3b). Next, we explored whether gut dysfunction was associated with an alteration of ENS connectivity. Analysis of an IF staining of the colon myenteric plexus revealed a significant decrease of Tuj1-IR neuronal processes, but no change in the number of HuC/D-IR neurons in Aβ-injected mice (Fig. 3c–e), suggesting an alteration of neuronal connectivity. Moreover, IF staining revealed that ChAT, but not nNOS, was reduced in mice injected with Aβ relative to controls (Fig. 3f and Supplementary Fig. 5a). Furthermore, connectivity proteins EphB2 and synaptophysin as well as downstream signaling molecules ERK and phospho-ERK were significantly lowered in Aβ-injected mice (Fig. 3g,h). Altogether, this data support mechanisms, also observed in vitro, that Aβ causes lesions of ENS through a degradation of enteric neuronal connectivity proteins and depletion of key neurotransmitter enzymes involved in gut motility.

To further explore the cross-species relevance of our findings in human, we next examined the Aβ capacity to cause ENS lesions in human complex organoids derived from iPSCs. We generated human iPSC-derived intestinal organoids (HIO) with an embedded neural crest cells (NCCs)-derived ENS (Supplementary Fig. 5b) [28]. After 24 h exposure of HIO to 1 µM Aβ, we observed an accumulation of Aβ at the vicinity of Tuj1-IR structures, but also localized at proximity to other cell types within the HIO (Fig. 3i,j). Importantly, to demonstrate that Aβ access to Tuj1-IR cells causes ENS lesions, we measured connectivity proteins after a dose-

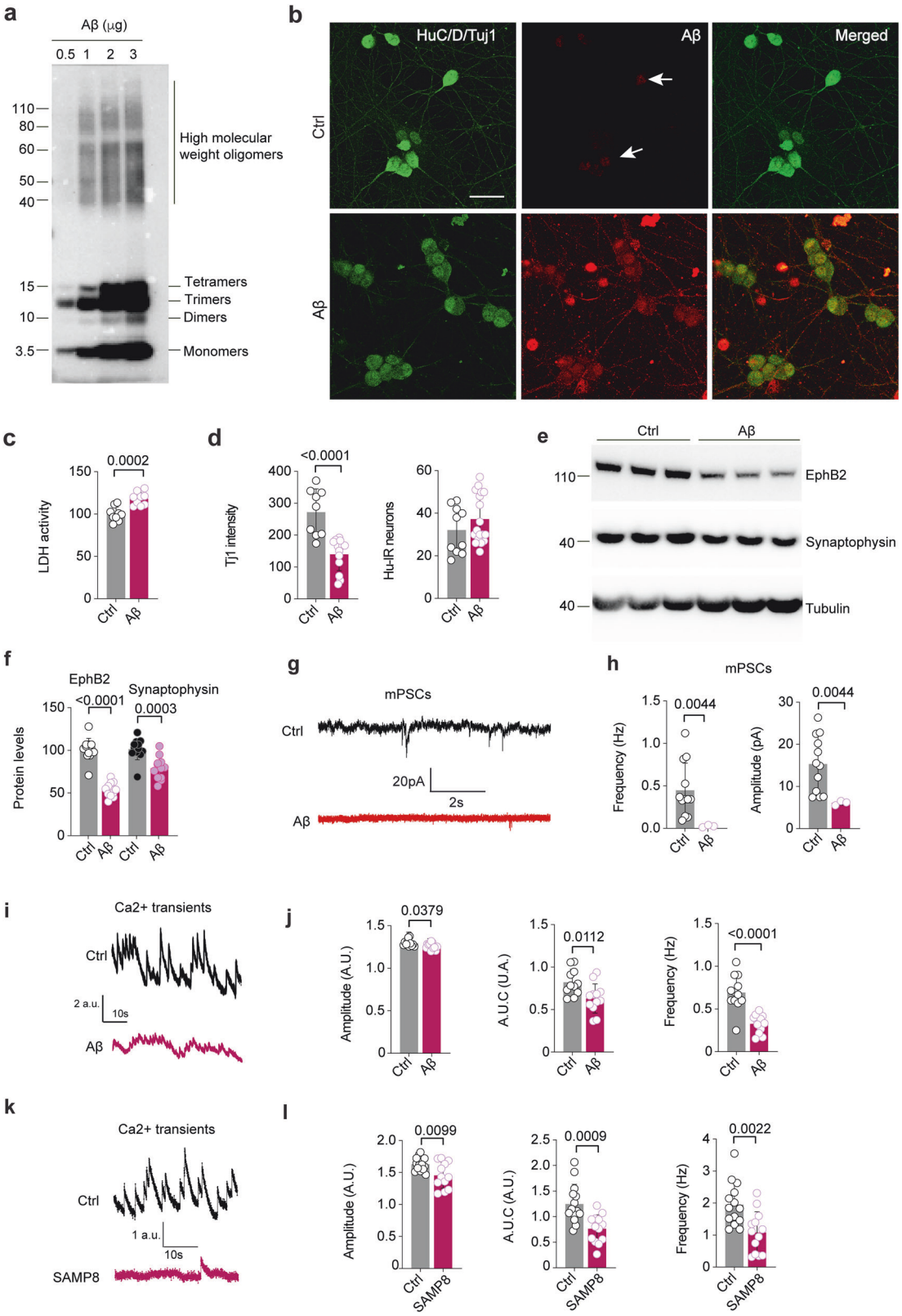

response to Aβ. Interestingly, we also observed a significant decrease of EphB2 and synaptophysin in HIO exposed to Aβ relative to controls (Fig. 3k and Supplementary Fig. 5c). This data suggest that Aβ impairs ENS connectivity in an in vitro intestinal model and clearly demonstrates Aβ capacity to cause ENS lesions in human intestinal organoids, which is in agreement with a recent study showing that Aβ alters neuronal connectivity in cerebroids [39].

To further confirm Aβ pathogenic activity in humans, we performed similar experiments using organotypic cultures of human colonic explants, which allows to maintain a near in vivo environment in a limited period of time [40, 41]. We first

Fig. 2 Aβ impairs the connectivity and activity of enteric neurons. a Immunoblot profil of synthetic Aβ preparation containing monomers, dimers, trimers, tetramers and high molecular weight oligomers. **b** IF staining of HuC/D, Tuj1 (green) and Aβ (red) in Ctrl and Aβ-treated pure enteric neurons isolated from WT rat. Scale bar, 20 μm. **c** LDH measures in culture media from cell cultures in **b**. Mann-Whitney (n = 9 well per condition from 3 independent cultures). **d** Quantification of Tuj1 and HuC/D IF signals from **b**. Mann-Whitney test. **e** Immunoblot of EphB2, synaptophysin (SYN) and β-tubulin in lysates of Ctrl and Aβ-treated pure enteric neurons isolated from WT rat. **f** Quantification of EphB2, synaptophysin proteins from **e**. Mann-Whitney (n = 9–12 well per condition). **g** Representative traces of spontaneous mPSC recorded from Ctrl or Aβ-treated ENS cultures isolated from WT rats. **h** Quantification of mPSCs amplitude and frequency from **f**. Mann–Whitney (n = 3–12 neurons per condition). **i** Representative traces of Ca^{2+} transients recorded in pure enteric neurons cultured from WT rat and treated with Aβ or sham (Ctrl). **j** Quantification of AUC, amplitude and frequency of Ca^{2+} transients obtained in **i**. Mann-Whitney (n = 11–12 well per condition). **k** Representative traces of Ca^{2+} transients recorded from pure enteric neurons isolated from Ctrl and SAMP8 mice. **l** Quantification of AUC, amplitude and frequency of Ca^{2+} transients obtained in **k**. Mann-Whitney (n = 12–14 well per condition).

established that explants cultured for 24 h still maintain neuronal cell structural integrity and viability (Supplementary Fig. 5d). We further demonstrated that colon explants expressed EphB2, synaptophysin, APP, PGP9.5, actin, PS1 and BACE1, but did not detect endogenous Aβ (Supplementary Fig. 5e). Interestingly, incubation of colonic explants with Aβ for 24 h significantly decreased EphB2, synaptophysin and PGP9.5 expression (Fig. 3l) and increased LDH release in the culture medium (Fig. 3m), indicating that Aβ impairs ENS connectivity and exerts a cytotoxicity in a fully mature and integrated human intestinal model.

Butyrate prevents Aβ-induced impairments of enteric neuronal function

We have previously shown that butyrate is a potent modulator of ENS and motility, acting in particular by increasing ChAT expression in enteric neurons and promoting colonic motility in rats [42]. Based on these beneficial properties of butyrate, we hypothesized that butyrate could restore Aβ-induced ENS connectivity and gut dysfunction. First, we examined whether butyrate can modulate basal levels of ENS connectivity proteins and enzymes involved in APP metabolism. Treatment of ENS cultures with butyrate dose-dependently increased EphB2 and synaptophysin (Supplementary Fig. 6a,b). Importantly, we showed that butyrate induced a dose-dependent decrease of APP, BACE1 and PS1 proteins (Supplementary Fig. 6c,d).

Next, we determined the capacity of butyrate to block neuronal alterations observed in SAMP8 mice. To this end, we treated pure enteric neurons isolated from SAMP8 mice with butyrate in vitro. IF staining showed that Tuj1-IR neuronal processes were significantly decreased in neurons isolated from SAMP8 mice and butyrate prevented these alterations as SAMP8 neurons treated with butyrate showed similar levels of Tuj1 as compared with Ctrl condition (Fig. 4a). In addition, the depletion of connectivity proteins EphB2 and synaptophysin observed in ENS cultures obtained from SAMP8 mice was blocked by butyrate, further validating its beneficial effects on neuronal connectivity.

To demonstrate whether butyrate can directly modulate Aβ-induced alterations on neuronal connectivity. We treated pure enteric neurons isolated from WT rats with exogenous Aβ in combination with butyrate. Again, Aβ caused a loss of Tuj1-IR neuronal processes and butyrate blocked these alterations (Supplementary Fig. 7a,b). Moreover, we incubated ENS cultures with Aβ for 24 h in combination with a butyrate dose-response. Remarkably, butyrate prevented Aβ-induced depletion of EphB2 and synaptophysin in a dose-dependent manner (Supplementary Fig. 7c,d). We reasoned that butyrate could indirectly restore levels of connectivity proteins by reducing Aβ, thereby limiting its access to synaptic proteins and their degradation. IF staining showed increased Aβ levels in enteric neurons isolated from SAMP8 mice (Fig. 4c). Strikingly, butyrate drastically reduced Aβ levels in SAMP8 neurons to that of Ctrl neurons.

This was further confirmed by ELISA measures revealing decreased concentrations of $Aβ_{1-40}$, $Aβ_{1-42}$ and total Aβ (Fig. 4d), associated with a reduced LDH release in the culture medium of SAMP8 neurons treated with butyrate (Fig. 4e). Furthermore, butyrate reduced exogenous Aβ in exposed enteric neurons (Supplementary Fig. 7e), suggesting an improved clearance since exogenous Aβ is in excess relative to endogenous Aβ. Together, these data suggest that butyrate preserves neuronal connectivity by reducing Aβ production and increasing its clearance, thus limiting its access to enteric neurons and mitigating subsequent ENS lesions.

Next, we aimed to determine the butyrate capacity to restore/modulate Aβ-induced changes in Ca^{2+} activity in enteric neurons as reported in Fig. 2. As expected, Aβ significantly reduced spontaneous Ca^{2+} activity as shown by example traces of spontaneous Ca^{2+} transients (Fig. 4f) and quantitative analysis of spontaneous Ca^{2+} transients showing decreased AUC and amplitude (Fig. 4g) in pure enteric neurons isolated from SAMP8 mice. Strikingly, butyrate prevented these alterations as Ca^{2+} transients were similar in SAMP8 neurons treated with butyrate and Ctrl neurons. Butyrate also rescued spontaneous Ca^{2+} transients in enteric neurons exposed to exogenous Aβ (Fig. 4h) by restoring AUC and amplitude to control levels (Fig. 4i). Furthermore, butyrate preserved veratridine-evoked Ca^{2+} transmission in SAMP8-derived enteric neurons (Supplementary Fig. 7f,g) and in WT rat-derived enteric neurons treated with exogenous Aβ (Supplementary Fig. 7h,i) as it restored AUC and amplitude of Ca^{2+} signals to control levels in both conditions. Together, these data indicate that butyrate alleviates Aβ-induced alteration of ENS connectivity and Ca^{2+} signaling in vitro.

Butyrate reduces APP amyloidogenic processing and ameliorates cholinergic phenotype in the gut of SAMP8 mice

Based on the overall in vitro findings demonstrating the capacity of butyrate to modulate Aβ production and ultimately restore enteric neuron connectivity, we next explored its capacity to prevent Aβ accumulation, modulate APP metabolism and ultimately ameliorate neuronal connectivity in the gut of SAMP8 mice. To this end, butyrate was administered daily via drinking water to 3-week-old weaned SAMP8 mice and controls (Fig. 5a). Metabolomic quantification showed an increased uptake of butyrate that translated to a significant decrease of butyrate in fecal contents, in line with previous studies reporting that butyrate upregulates MCT1 transporters to foster its uptake by intestinal epithelial cells [43, 44] (Supplementary Fig. 8a). We observed no difference in total weight and water content of the fecal pellets of SAMP8 mice relative to controls and butyrate treatment did not modify these outcome measures (Supplementary Fig. 8b–d). Interestingly, in butyrate-treated SAMP8 mice (SAMP8 +), IF staining showed a significant decrease in Aβ accumulation in colonic myenteric plexus as compared with non-treated SAMP8 (SAMP8) (Supplementary Fig. 9a). These results were confirmed by ELISA assay showing a significant decrease of $Aβ_{1-40}$ and $Aβ_{1-42}$ in the colon (Fig. 5b,c) and plasma (Fig. 5d) of SAMP8+ relative to SAMP8 mice. Since the steady-state levels of Aβ are determined by the balance between its production and clearance, we measured APP processing and neprilysin in the colon. Expression levels of APP, BACE1, but not PS1, were increased in the colon of SAMP8 as compared with Ctrl mice, whereas neprilysin was decreased (Fig. 5e and Supplementary Fig. 9b), confirming a catabolic shift

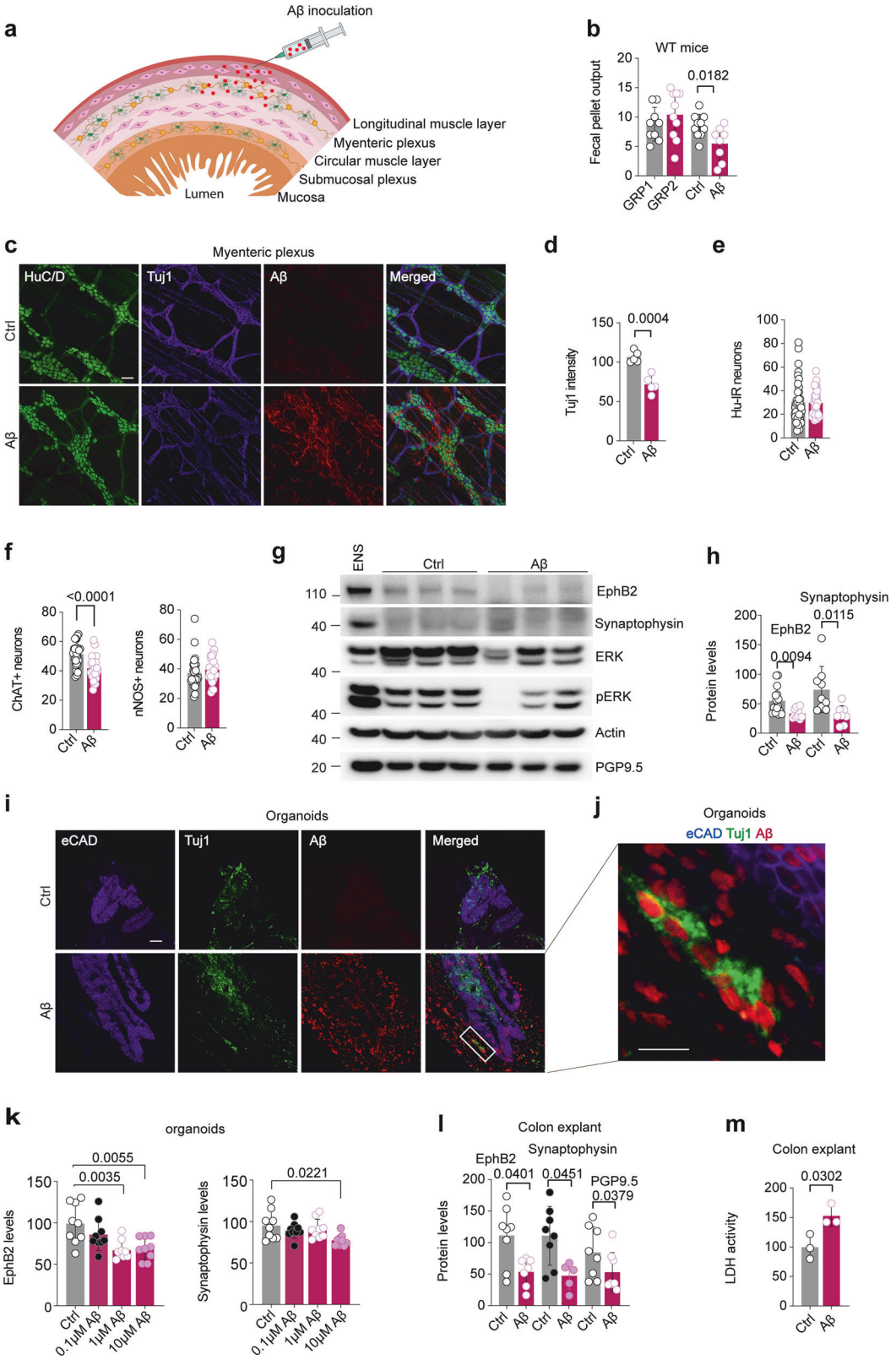

towards an amyloidogenic processing of APP. Most importantly, expression levels of these proteins were similar between SAMP8 treated with butyrate and Ctrl mice. Furthermore, BACE1 activity was significantly reduced in SAMP8+ mice relative to SAMP8 (Fig. 5f). These results indicate that butyrate reduces Aβ accumulation in the gut and brain by modulating APP metabolism.

We have previously shown that butyrate enema significantly increases the phenotype of nNOS+ and ChAT+ myenteric neurons in vivo [42, 45]. Therefore, we examined whether butyrate restores

Fig. 3 Aβ affects ENS connectivity and GI function in mouse and human models. a Schematic depicting intramuscular injection of Aβ or saline in the colon longitudinal muscle layer and myenteric plexus of 3mo WT mice and subsequent analysis 1 month later. **b** FPO measures during 2 h in mice from **a**. GRP1, cohort before saline injection; GRP2, cohort before Aβ injection. Mann-Whitney (n = 8–10 animals per condition). **c** IF staining of HuC/D (green), Tuj1 (purple) and Aβ (red) in colon myenteric plexus of mice from **a**. Scale bar, 50 μm. (**d,e**) Quantification of HuC/D (**d**) and Tuj1 (**e**) IF signals from **c**. Mann-Whitney (n = 5–6 animals per condition). **f** Quantification of ChAT and nNOS IF signals measured in colon myenteric plexus of mice from **a**. Mann-Whitney (n = 5–6 animals per condition). **g** Immunoblots of indicated proteins in whole colon lysates of mice in **a**. **h** Quantification of EphB2 and synaptophysin proteins from **g**. Mann-Whitney (n = 8–15 mice per condition). **i** IF staining of eCAD (purple), Tuj1 (green) and Aβ (red) in Ctrl and Aβ-treated HIO + ENS. Scale bar, 100 μm. **j** Higher magnification of image representing the boxed area in **i**. Scale bar, 10 μm. **k** Quantification of EphB2 and synaptophysin proteins in HIO + ENS from **i**. Kruskal-Wallis and Dunn's multiple comparisons (n = 9 HIO + ENS per condition). **l** Quantification of EphB2, synaptophysin and PGP9.5 proteins in lysates of Ctrl and Aβ-treated human colon explants cultured for 24 h. Mann–Whitney (n = 5-8 colon explants per condition). **m** LDH measure in culture media conditioned from Ctrl and Aβ-treated human colon explants cultured for 24 h. Mann-Whitney (n = 3 colon explants per condition).

nNOS and ChAT expressions and connectivity of myenteric enteric neurons in SAMP8 mice. As expected, nNOS and ChAT expression were significantly reduced in SAMP8 relative to Ctrl mice (Fig. 5g,h). Importantly, expression of ChAT, but not nNOS, was restored in myenteric enteric neurons of SAMP8+ mice. Furthermore, Tuj1-IR interganglionic fiber tracts, which were reduced in SAMP8 myenteric plexus, were restored to control levels in SAMP8+ mice with no changes in the overall number of HuC/D+ enteric neurons (Fig. 5i and Supplementary Fig. 9c). These data suggest that butyrate ameliorates myenteric cholinergic phenotype and preserves interganglionic fibers in SAMP8 mice.

Next, to explore a potential mechanism of action, we examined butyrate modulation of histone deacetylase activity in the colon of SAMP8 mice. We observed abnormal expressions of HDAC1 and HDAC3, but not HDAC2, associated with a hyperacetylation of histone 3 and histone 4 on lysine 9 and lysine 16, respectively, in SAMP8 mice relative to controls (Supplementary Fig. 10a–h). Most importantly, butyrate treatment prevented these abnormalities. Thus, butyrate might exert its beneficial effects, at least partially, through a modulation of HDAC function.

Butyrate ameliorates gut neuroinflammation in SAMP8 mice

A large population of astrocyte-like enteric glial cells (EGCs) populates gut muscle layers and the intestinal mucosa. In response to mediators/factors or stressor originating from the gut environment, particularly during inflammation, EGCs become reactive in a similar fashion to astrogliosis occurring in the brain in response to injury or pathological insults [46]. The glial fibrillary acidic protein (GFAP) is expressed by EGCS, represents an excellent index of enteric gliosis response to inflammation and interestingly, is increased in the colon of Parkinson's disease patients [47]. Thus, we examined GFAP-immunoreactive (IR) EGCs and butyrate capacity to reduce enteric gliosis in SAMP8 mice. IF staining of GFAP revealed greater numbers and larger areas of GFAP-IR EGCs with enlarged soma in the myenteric plexus of the colon from SAMP8 mice (Fig. 6a,b). Importantly, butyrate lowered reactive EGCs as shown by the decreased density of GFAP-IR EGCs, and the smaller area of GFAP immunoreactivity in SAMP8+ mice. Together, these data indicate that butyrate drastically diminishes peripheric gliosis in the context of accumulating Aβ.

Previous studies established that different species of Aβ aggregates could induce a glial activation and the production of proinflammatory cytokines to harm neurons [48], a process which in turn, can suppress the phagocytosis and clearance of Aβ by glia, thus fueling its accumulation through a vicious cycle [49]. To further explore whether gliosis is associated with an increase in neuroinflammation, we measured transcript levels of selected inflammatory immune factors. Cytokines measured from colon tissues were drastically elevated in SAMP8 mice, particularly Tumor Necrosis Factor α (TNFα) and interleukin 6 (IL6) with a 3-fold and 10-fold increase of mRNA levels, respectively, which were reversed to control levels in SAMP8+ mice (Fig. 6c,d). However, IL1β and Interferon γ (INFγ) did not differ between groups. IL10, an anti-inflammatory cytokine, showed a trend toward an increase without reaching statistical significance. These data indicate that SAMP8 mice display a systemic pro-inflammatory state in the context of aging and accumulating amyloid and that butyrate ameliorated gut neuroinflammation.

Butyrate ameliorates neuronal connectivity and prevents gut-brain dysfunctions in SAMP8 mice

Since butyrate blocked Aβ accumulation and ameliorated multiple Aβ-associated phenotypes in SAMP8 mice, we first examined levels of ENS connectivity proteins EphB2 and synaptophysin. As expected, EphB2 and synaptophysin were significantly reduced in myenteric neurons. However, expression levels of these proteins were restored to control levels in the colon of SAMP8+ mice with no changes in overall PGP9.5 neuronal marker (Fig. 7a,b and Supplementary Fig. 11a).

Next, we investigated the functional consequences of butyrate-induced amelioration of ENS connectivity. We found that FPO was reduced in SAMP8 relative to Ctrl mice, but restored in SAMP8+ mice (Fig. 7c). Moreover, butyrate treatment did not affect body weight (Supplementary Fig. 11b) and intestinal length (Supplementary Fig. 11c). Taken together, these data suggest that butyrate preserves the expression of ENS connectivity proteins and ameliorates spontaneous contractile function of the gut.

Next, we examined whether butyrate ameliorates AD-related brain function, particularly memory. In the NOR test, as expected, memory was disrupted in SAMP8 mice compared with Ctrl littermates. However, memory was restored in SAMP8+ as they performed at Ctrl levels in the novel object task (Fig. 7d). To ensure that butyrate beneficial effects observed in the NOR test are robust and can be replicated with an additional and distinct memory test, we used the Y-maze. SAMP8+ mice showed significantly greater alternations in the Y-maze test relative to SAMP8 mice and performed equally to Ctrl mice (Fig. 7e). The number of arm entries was similar between groups. This indicates that butyrate ameliorated the short-term memory deficit in SAMP8 mice. In sharp contrast, disinhibition and ambulatory hyperactivity phenotypes were not rescued as SAMP8 and SAMP8+ mice performed equally, but poorly relative to Ctrl counterparts as they spent more time in the open arms of the EPM (Fig. 7f) and traveled a greater distance in the OF (Fig. 7g). Collectively, these results demonstrate that butyrate prevents ENS dysconnectivity and memory deficit in SAMP8 mice.

Butyrate prevents brain amyloid pathology in SAMP8 mice

We aimed to investigate the impact of butyrate on amyloid pathology in the brain. First, we examined overall neuronal architecture in the CNS of SAMP8 mice. In the hippocampus, a vulnerable brain region in AD, we assessed neuronal density in the granule cells layer of the dentate gyrus (DG) by using a broad and specific neuronal marker Neuronal Nuclear antigen (NeuN). We found no difference in cell density in SAMP8 relative to control mice (Supplementary Fig. 12a,b). Moreover, at molecular level, we

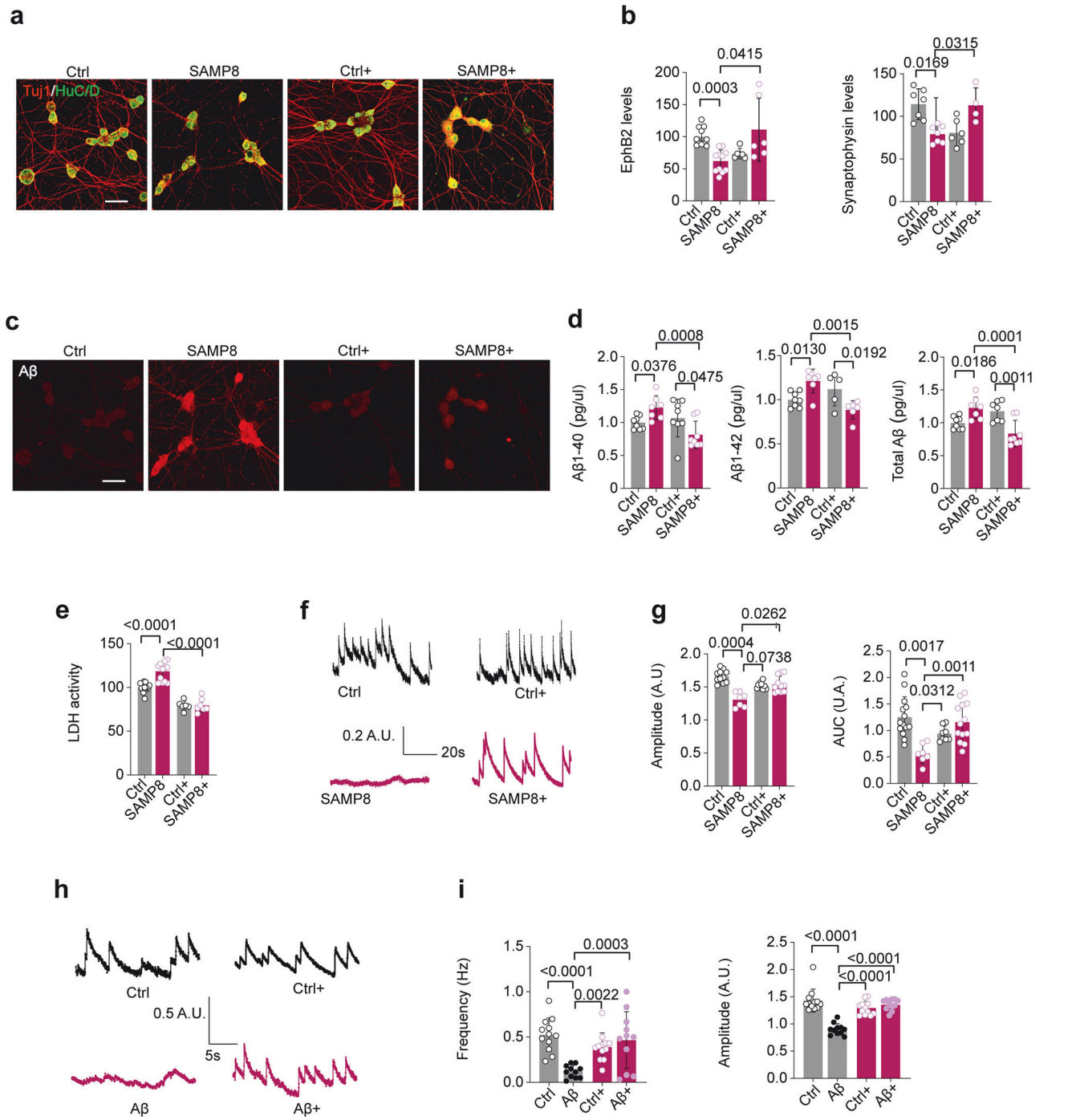

Fig. 4 Butyrate protects enteric neurons against Aβ. a IF staining of HuC/D (green) and Tuj1 (red) in pure enteric neurons isolated from Ctrl and SAMP8 that were treated with butyrate (+) or sham in vitro. Scale bar, 20 µm. **b** Quantification of EphB2 and synaptophysin immunoblots of ENS cultures isolated from Ctrl and SAMP8 mice and treated with butyrate (+) or sham in vitro. Two-way ANOVA and Tukey's multiple comparisons (n = 11–12 animals per condition). **c** IF staining of Aβ (red) in ENS cultures from **a**. Scale bar, 20 µm. **d** ELISA quantification of Aβ levels in media conditioned from pure enteric neurons cultures from **b**. Two-way ANOVA and Tukey's multiple comparisons (n = 5–7 animals per condition). **e** LDH measure in media conditioned from pure enteric neurons cultures from **b**. Two-way ANOVA and Tukey's multiple comparisons (n = 6–13 animals per condition). **f** Example traces of Ca^{2+} transients recorded in pure enteric neurons isolated from Ctrl and SAMP8 mice and treated in vitro with butyrate (+) or sham. **g** Quantification of amplitude and AUC of Ca^{2+} transients from **f**. Two-way ANOVA and Tukey's multiple comparisons (n = 8–15 wells per condition). **h** Example traces of Ca^{2+} transients recorded in pure enteric neurons isolated from WT rats and treated with butyrate (+) and Aβ in vitro. **i** Quantification of amplitude and AUC of Ca^{2+} transients from **h**. Two-way ANOVA and Tukey's multiple comparisons (n = 8–15 wells per condition).

found a decrease in expression levels of EphB2 and synaptophysin in the hippocampus of SAMP8 relative to Ctrl mice (Fig. 8a and Supplementary Fig. 12c). Interestingly, expression of EphB2, but not synaptophysin, was preserved in SAMP8+ mice.

Next, we explored butyrate effect on brain neuroinflammation. GFAP is commonly used as marker of abnormal activation and proliferation of astrocytes due to neuronal brain damage, also known as astrogliosis [50]. Astrogliosis has been observed around

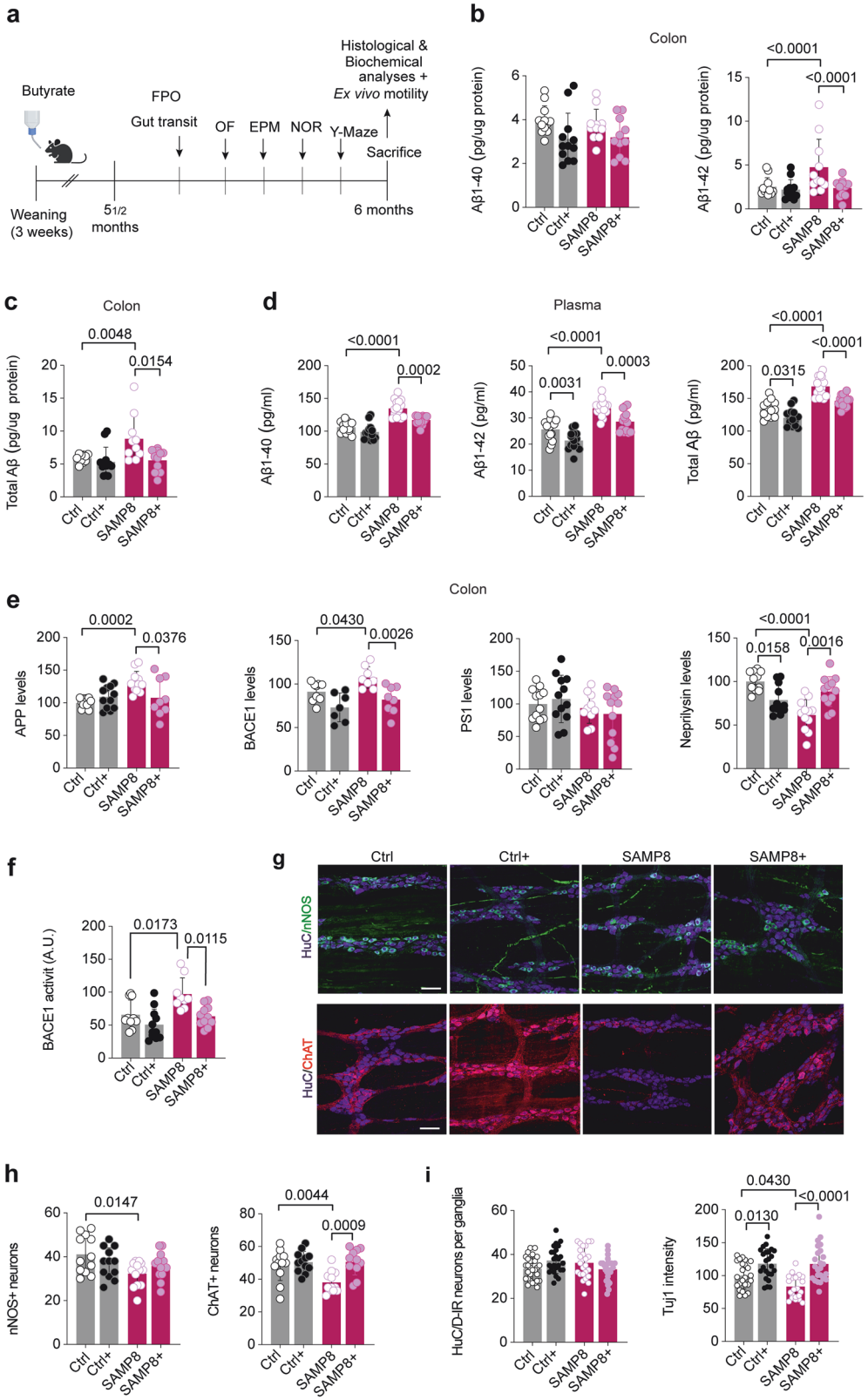

Aβ plaques from the prodromal stages of AD and GFAP expression has been reported to correlate with Aβ plaque density in AD brain tissue [51]. Noticeably, in the hippocampus, GFAP-IR glial cells reactivity was significantly increased in the hilus-CA1 region of SAMP8 compared with Ctrl mice and markedly reduced in SAMP8+ relative to SAMP8 mice (Fig. 8b,c). Measure of transcript levels of selected inflammatory immune factors revealed that TNFα was markedly and unexpectedly reduced in SAMP8 mice as compared with Ctrl mice and restored to control levels in SAMP8+ (Supplementary Fig. 12d,e). Although INFγ and IL6 did not differ between SAMP8 and Ctrl mice, they were significantly reduced in SAMP8+ mice. IL1β and IL10 were similar between

Fig. 5 butyrate reduces Aβ production and improves cholinergic connectivity in SAMP8 mice. a Experimental design of Ctrl and SAMP8 mice supplemented with butyrate in drinking water (+) or water for 5 months and subsequent analyses. (**b**–**d**), ELISA quantification of Aβ levels in whole colon lysates (**b,c**) and plasma (**d**) of mice from **a**. Two-way ANOVA and Tukey's multiple comparisons (n = 10–15 animals per group). **e** Quantification of indicated proteins obtained from immunoblots of whole colon lysates of mice from **a**. Two-way ANOVA and Tukey's multiple comparisons (n = 7–12 animals per group). **f** BACE1 activity measured in colon lysates of mice from **a**. Values are represented as arbitrary units (AU). Two-way ANOVA and Tukey's multiple comparisons (n = 9–11 animals per group). **g** IF staining of HuC/D (purple), ChAT (red) and nNOS (green) in colon myenteric plexus of Ctrl and SAMP8 mice in **a**. Scale bar, 50 μm. **h** Quantification of nNOS and ChAT IF signals from **g**. Two-way ANOVA and Tukey's multiple comparisons (n = 5–8 mice per group). **i** Quantification of HuC/D and Tuj1 IF signals from **a**. Two-way ANOVA and Tukey's multiple comparisons (n = 5–8 mice per group).

SAMP8 and Ctrl mice and unaffected by butyrate treatment in either group.

A measure of Aβ levels by ELISA assay revealed an increase of total Aβ and $Aβ_{1-42}$, but not $Aβ_{1-40}$, in the hippocampus. Importantly, butyrate reduced Aβ to Ctrl levels in SAMP8+ mice (Fig. 8d). To determine whether Aβ plaques are formed in the hippocampus of SAMP8 mice, we used the amyloid dye thioflavin S (TS) for histological staining, which allows a quantification of Aβ burden but has the disadvantage of assessing only larger accumulations of aggregated Aβ. We found no TS-stained plaque-like structures in SAMP8 mice (Supplementary Fig. 12f), consistent with reports that Aβ plaques are only detected in the brain between 16-18 months of age in this model [52].

Lastly, we examined the butyrate capacity to block the amyloidogenic processing of APP in the hippocampus. We found that BACE1 and PS1 expression levels were increased in SAMP8 as compared with Ctrl mice (Fig. 8e and Supplementary Fig. 12g). Importantly, butyrate prevented an increase of these proteins in SAMP8 + , which displayed levels similar to that in Ctrl mice. In contrast, there was no difference in APP and neprilysin proteins expression between groups. Altogether, these data demonstrate that butyrate ameliorated several key aspects of amyloid pathology in the brain of SAMP8 mice.

DISCUSSION

The gut is increasingly recognized as a key organ in AD aetiology and physiopathology [31]. However, physiopathological processes underlying gut dysfunctions and therapies remain ill-defined. Here, we show early Aβ-induced alterations of ENS connectivity and gut function prior to memory decline in SAMP8 mice. An abnormal Aβ metabolism, involving increased anabolism and decreased catabolism, causes its excessive production and subsequent alterations of ENS connectivity and gut function. Exposure of various in vitro models and WT mice to exogenous Aβ mimics ENS alterations and gut dysfunctions seen in SAMP8 mice. Remarkably, an early supplementation of butyrate to SAMP8 mice at weaning blocks Aβ accumulation, neuroinflammation and prevents ENS dysconnectivity and gut-brain dysfunctions. Thus, butyrate-based intervention may hold potential for new disease-modifying therapies in AD.

Gastrointestinal function relies on the integrated interaction and activity of a variety of cell types including enteric neurons and glial cells that form the intrinsic circuits of the ENS [53]. Perturbation of these interactions could underlie gastrointestinal disease onset and elicit variable degrees of abnormal gut function, pinpointing the ENS as a mediator in diseases of the gut [10]. We found that enteric neurons excessively produce Aβ, thereby altering ENS connectivity and subsequently causing gut dysfunction in SAMP8 mice. SAMP8 mice represent a model of sporadic AD, which accounts for 95% of the cases, and exhibit early onset pathologies associated to neurodegenerative changes reported in transgenic APP-overexpressing mouse models [21]. SAMP8 mice also develop amyloid plaques and display an accelerated aging, which is of great importance because age is the main risk factor of AD. In contrast, the majority of AD mouse models are developed to mimic the genetic cause of human AD, which represent 5% of cases, by overexpressing mutated forms of human APP, PS1/2, and/or Tau protein. We observe that SAMP8 mice exhibited less anxiety related behavior than controls at 2- and 6-months of age. A similar trend in tendency to spend more time in the open arms of elevated-plus maze was reported in 6-month-old SAMP8 mice relative to controls in a previous study [54]. The mechanistic link between anxiety and AD neuropathology remains unclear.

Interestingly, Aβ production is increased in the ENS in young pre-symptomatic SAMP8 mice, when there is no memory impairment, indicating that an early pathogenic process may facilitate gut amyloidosis. Thus, it is conceivable that ENS constitutes an entry point of Aβ pathology in early stages of the disease, at least in sporadic cases. Although the presence of Aβ in the gut and feces of AD mice was previously reported [54–56], our study sheds lights on molecular mechanisms contributing to its excessive production in ENS. Indeed, levels of APP and/or γ-secretase components were increased in the ENS of SAMP8 mice, as observed in APP/PS1 model [57]. In addition, our study revealed a decrease in neprilysin, a major Aβ-degrading enzyme [58], further fueling Aβ accumulation in the ENS by impaired clearance. However, the mechanism driving the dysregulation of Aβ metabolism remains unclear. Evidence in the literature suggests that gut microbiota could be involved. Indeed, gut dysbiosis contributes to amyloidosis in AD [59–61] and abnormal changes in SCFAs, which are consistently observed in AD mouse models and patients with AD [62, 63], could facilitate the amyloidogenic process in the ENS. Additionally, bacterial amyloids produced by gut microbes, may exacerbate host amyloid aggregation and contribute to gut amyloidosis [64, 65].

Aβ altered ENS connectivity by depletion of key synaptic proteins such EphB2 and synaptophysin, which are master regulators of ENS connectivity [16] and brain plasticity [15, 66], unveiling a "mirror effect" between the gut and the brain. Further, we showed that adding exogenous Aβ to distinct in vitro and in vivo models, including hIPSC-derived organoids and organotypic cultures of human colon, and WT mice altered ENS connectivity, supporting the notion that excessive Aβ productions by enteric neurons promotes a detrimental autocrine loop that impairs ENS connectivity and gut function as shown by a reduced FPO in WT mice injected with Aβ. Indeed, we found an impaired enteric network activity induced by Aβ, which could directly trigger adverse effects such as altered FPO in SAMP8 mice. This notion is reinforced by the demonstration that Hexamethonium, a nicotinic antagonist, blocked ENS networks activity and impaired colonic motility in mice [67]. Interestingly, a reduced FPO, which is consistent with an impaired colonic transit, is also seen in patients with AD [4], in particular in presymptomatic phases, supporting the need for development of an early diagnosis and therapies targeting ENS dysconnectivity to restore gut function.

We used 3-week-old SAMP mice and controls in order to counteract early ENS dysconnectivity and prevent gut dysfunction, which manifest before brain symptoms. Furthermore, we reasoned that butyrate will be more efficient when gut microbiota is not yet fully dysbiotic with a significant impact on amyloid production. Butyrate ameliorated several aspects of Aβ pathology, including ENS remodeling and gut dysfunction, in SAMP8 mice. Notably, butyrate displayed multiples activities that synergistically

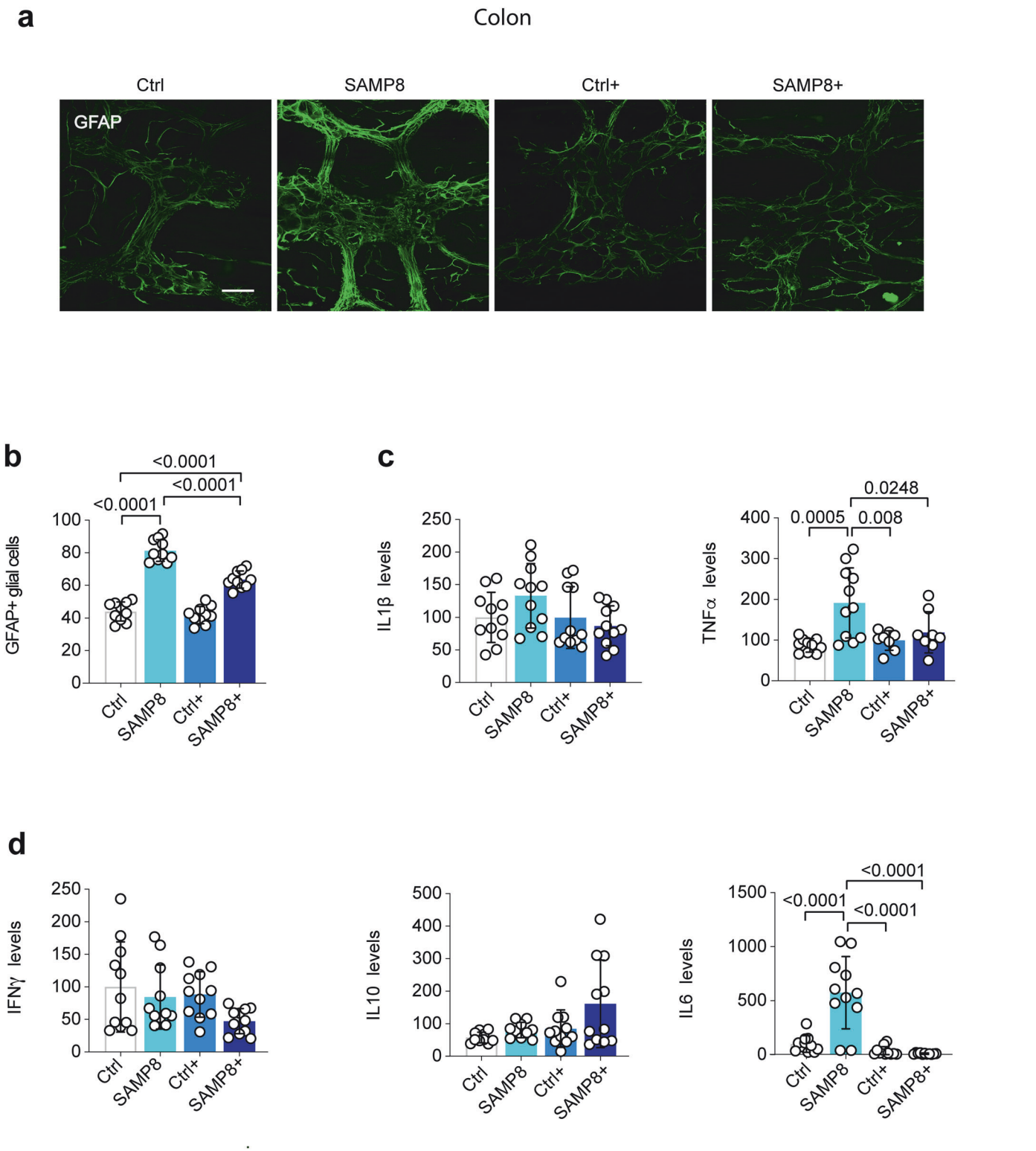

Fig. 6 Butyrate reduces gut neuroinflammation in SAMP8 mice. a IF staining of GFAP (green) in colon myenteric plexus of Ctrl and SAMP8 mice that received butyrate (+) or water. Scale bar, 50 μm. **b** Quantification of GFAP IF signals from **a**. Two-way ANOVA and Tukey's multiple comparisons (n = 10 mice per group). **c,d** RT-qPCR measures of indicated immune factors in the colon of Ctrl and SAMP8 mice treated with butyrate (+) or water. Two-way ANOVA and Tukey's multiple comparisons (n = 8–11 mice per group).

prevented ENS dysconnectivity and ultimately gut dysfunctions. Indeed, butyrate modulated: (1) Aβ metabolism; (2) ENS connectivity; (3) enteric neuromediators; and (4) neuroinflammation. Butyrate reduced Aβ production likely by downregulating APP and its cleaving amyloidogenic enzymes PS1 and BACE1 and increasing NEP expression. Although these modulations were reported in cell lines from the CNS [18], the description of such mechanisms in the ENS is unprecedented. Butyrate also improved ENS

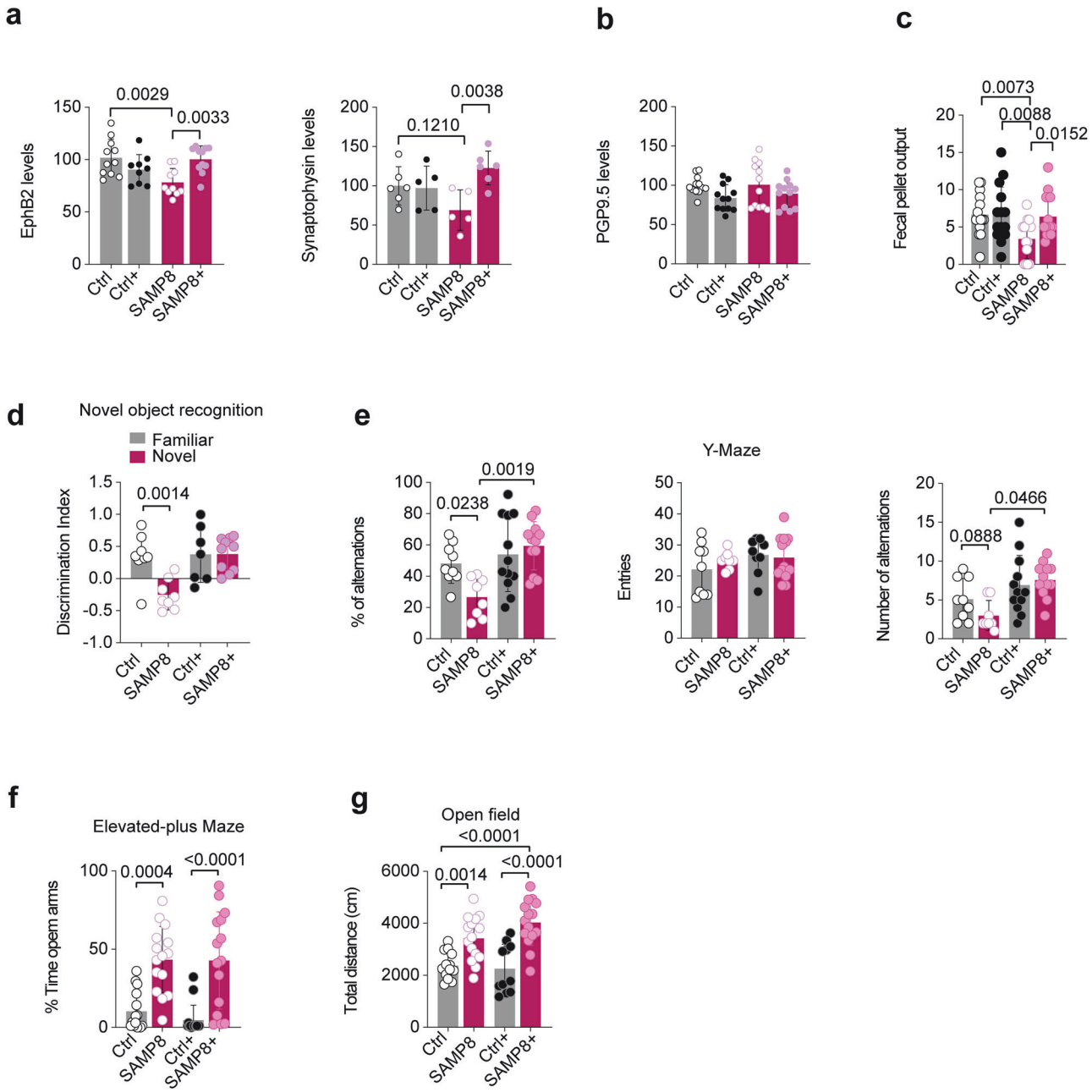

Fig. 7 Butyrate improves gut connectivity and motility in SAMP8 mice. a,**b**, Quantification of EphB2, synaptophysin (**a**) and PGP9.5 (**b**) proteins in colon of Ctrl and SAMP8 mice treated with butyrate (+) or water. Two-way ANOVA and Tukey's multiple comparisons (n = 5–6 animals per group). **c** FPO measured for 2 h of Ctrl and SAMP8 mice treated with butyrate (+) or water. Two-way ANOVA and Tukey's multiple comparisons (n = 14–15 mice per group). (**d**—**g**), NOR (**d**), Y-Maze (**e**), EPM (**f**) and OF (**g**) tests of Ctrl and SAMP8 mice treated with butyrate (+) or not. NOR, discrimination index differences were assessed with paired t-tests. Discrimination index of 0.5 indicates chance preference; Y-Maze, EPM and OF, Two-way ANOVA and Tukey's multiple comparisons (n = 8–15 mice per group).

connectivity by blocking Aβ-induced EphB2 and synaptophysin depletions, likely by transcriptional control of genes (see Supplementary Fig. 6) and/or limiting Aβ interaction with EphB2 and its subsequent depletion as described in CNS [15, 68, 69]. Furthermore, impairments of ChAT and nNOS phenotypes were prevented in the ENS, which contributes to an amelioration of gut functions as shown by a normalization of FPO in SAMP8 mice. This is consistent with our previous studies showing that butyrate ameliorates gut motility in rats [42]. Finally, butyrate reduced inflammation, a process known to promote amyloidosis [49], which may lower Aβ production and subsequent adverse effects on ENS connectivity and gut function. Indeed, butyrate lowered IL6, which has been shown to cause GI dysfunction in an irritable bowel syndrome mouse model [70], indicating that independently of its interconnection to Aβ pathology, reducing IL6 per se may ameliorates gut function. Altogether these pleiotropic effects of butyrate contribute to its overall beneficial effects on gut functions in SAMP8 mice. Oral butyrate has been shown to modulate the expression of different SCFA carriers, such as MCT1 in the intestinal tract, including the colon, and may involve interactions with the gut microbiota-secreted soluble factors [71, 72]. Butyrate may also activate vagal afferents and release gut hormones that might modulate intestinal transport [73]. Importantly, we also showed that butyrate prevented memory loss in

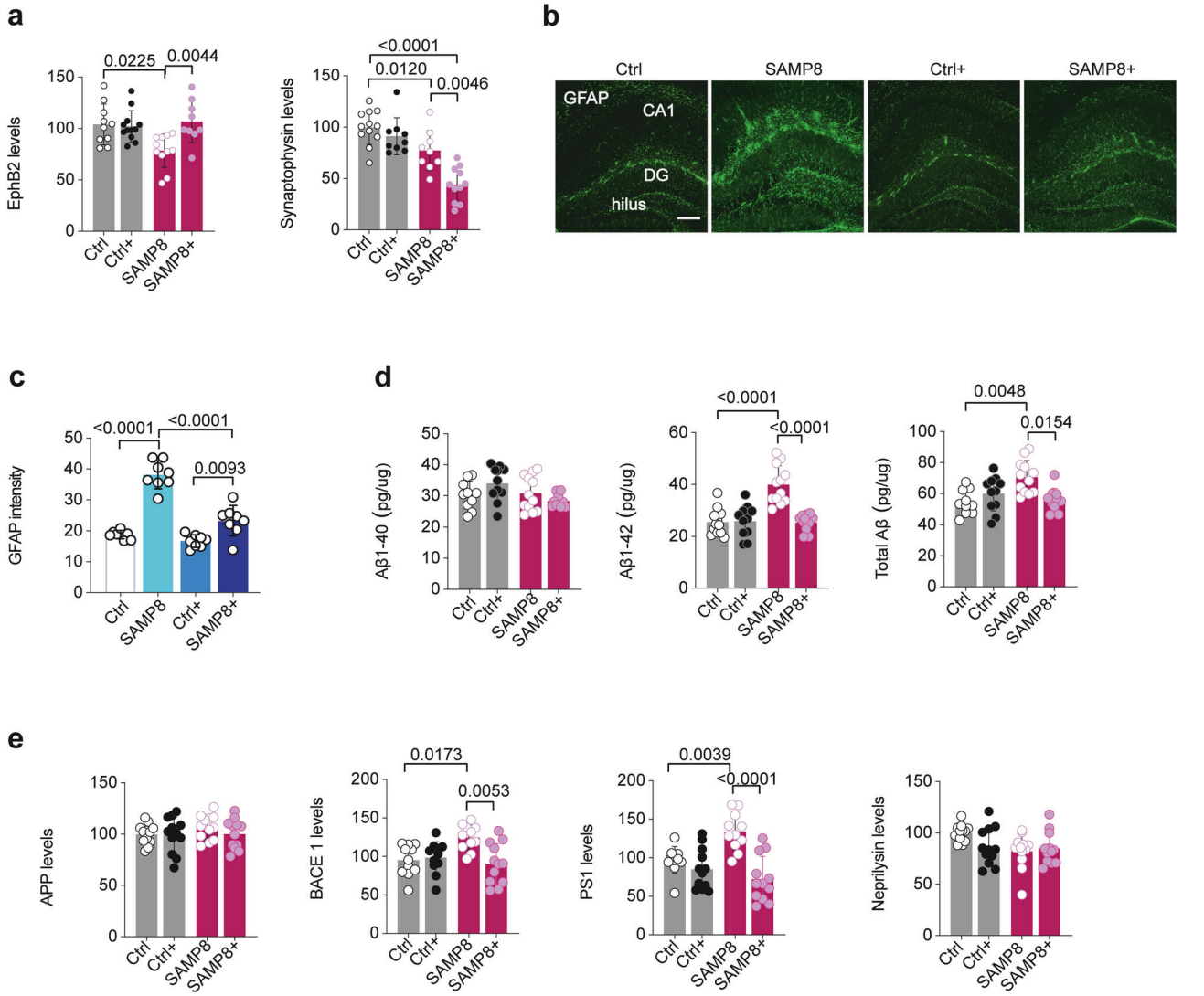

Fig. 8 Butyrate ameliorates amyloid pathology in the brain of SAMP8 mice. a Quantification of EphB2 and synaptophysin proteins in the hippocampus of Ctrl and SAMP8 mice treated with butyrate (+) or water. Two-way ANOVA and Tukey's multiple comparisons (n = 10–12 animals per group). **b** IF staining of GFAP (green) in the hippocampus of Ctrl and SAMP8 mice that received butyrate (+) or water. CA1, CA1 region; DG, Dentate gyrus. Scale bar, 50 μm. **c** Quantification of GFAP IF signals obtained from **c**. Two-way ANOVA with Tukey's multiple comparisons (n = 8 mice per group). **d** ELISA quantification of Aβ levels in the hippocampus of mice that received butyrate (+) or water. Two-way ANOVA and Tukey's multiple comparisons (n = 10–15 animals per group). **e** Quantification of indicated proteins obtained from immunoblots of hippocampal lysates of mice that received butyrate (+) or water. Two-way ANOVA and Tukey's multiple comparisons (n = 11–12 animals per group).

SAMP8 mice, which is consistent with previous studies conducted in distinct AD mice [20, 74]. We found that astrogliosis was selectively prominent in some area of the hippocampus such as the Hilus and CA1 region, but not the DG, which is supported by studies in pre-clinical models [75] and patients with AD [76].

A limitation of our study is that we did not assess the contribution of SAMP8 gut microbiota to amyloidosis. Indeed, bacteria populating the gut microbiota can release amyloids, such as curli fibrils, that stimulate peripheric inflammation and host amyloidogenic process [64]. Exploration of microbiota dysbiosis and its modulation of gut amyloid pathology and inflammation represent major mechanisms that are beyond the scope of the present study. Indeed, a multidisciplinary research approach incorporating large-scale patient cohort studies alongside pre-clinical models, omics technologies, and systems biology are needed for a comprehensive and thorough exploration of these mechanistic interplays in future studies.

Furthermore, it is unclear whether butyrate prevented memory by mitigating Aβ translocation from the gut into the brain via the vagus nerve or bloodstream. Further studies are warranted to better understand aspects of microbiota contribution and gut to brain amyloid propagation. We did not assess butyrate capacity to reverse Aβ pathology at advanced stages of the disease when gut and brain symptoms are fully blown because our study focused on a prevention paradigm. However, a previous study showed butyrate capacity to restore memory at an advanced stage of pathology [77].

In summary, our study supports the notion that Aβ plays a pivotal role in ENS dysconnectivity and gut dysfunction in AD. Butyrate counteracts Aβ-mediated enteric neuropathies and significantly improves major gut and brain dysfunctions, indicating that butyrate may hold promise as therapeutic agent. Further studies are warranted to determine whether slowing or preventing pathogenic cascades towards dementia can be achieved by using prebiotics, probiotics and fiber-enriched diet to promote butyrate uptake.

DATA AVAILABILITY

The data will be made available upon reasonable request to the corresponding author.

REFERENCES

1. Hampel H, Hardy J, Blennow K, Chen C, Perry G, Kim SH, et al. The amyloid-beta pathway in Alzheimer's disease. Mol Psychiatry. 2021;26:5481–503.
2. Tortajada-Soler M, Sanchez-Valdeon L, Blanco-Nistal M, Benitez-Andrades JA, Liebana-Presa C, Bayon-Darkistade E. Prevalence of comorbidities in individuals diagnosed and undiagnosed with Alzheimer's Disease in Leon, Spain and a proposal for contingency procedures to follow in the case of emergencies involving people with Alzheimer's Disease. Int J Environ Res Public Health. 2020;17:3398.
3. Browne J, Edwards DA, Rhodes KM, Brimicombe DJ, Payne RA. Association of comorbidity and health service usage among patients with dementia in the UK: a population-based study. BMJ Open. 2017;7:e012546.
4. Nedelec T, Couvy-Duchesne B, Monnet F, Daly T, Ansart M, Gantzer L, et al. Identifying health conditions associated with Alzheimer's disease up to 15 years before diagnosis: an agnostic study of French and British health records. Lancet Digit Health. 2022;4:e169–78.
5. Kang J, Lee M, Park M, Lee J, Lee S, Park J, et al. Slow gut transit increases the risk of Alzheimer's disease: An integrated study of the bi-national cohort in South Korea and Japan and Alzheimer's disease model mice. J Adv Res. 2024;65:283–95.
6. Nakase T, Tatewaki Y, Thyreau B, Mutoh T, Tomita N, Yamamoto S, et al. Impact of constipation on progression of Alzheimer's disease: A retrospective study. CNS Neurosci Ther. 2022;28:1964–73.
7. Comi C, Magistrelli L, Oggioni GD, Carecchio M, Fleetwood T, Cantello R, et al. Peripheral nervous system involvement in Parkinson's disease: evidence and controversies. Parkinsonism Relat Disord. 2014;20:1329–34.
8. Polis B, Samson AO A New perspective on Alzheimer's Disease as a brain expression of a complex metabolic disorder. In: Wisniewski T (ed). *Alzheimer's Disease:* Brisbane (AU), 2019.
9. Furness JB. The enteric nervous system and neurogastroenterology. Nat Rev Gastroenterol Hepatol. 2012;9:286–94.
10. Holland AM, Bon-Frauches AC, Keszthelyi D, Melotte V, Boesmans W. The enteric nervous system in gastrointestinal disease etiology. Cell Mol Life Sci. 2021;78:4713–33.
11. Semar S, Klotz M, Letiembre M, Van Ginneken C, Braun A, Jost V, et al. Changes of the enteric nervous system in amyloid-beta protein precursor transgenic mice correlate with disease progression. J Alzheimers Dis. 2013;36:7–20.
12. Joachim CL, Mori H, Selkoe DJ. Amyloid beta-protein deposition in tissues other than brain in Alzheimer's disease. Nature. 1989;341:226–30.
13. Mucke L, Selkoe DJ. Neurotoxicity of amyloid beta-protein: synaptic and network dysfunction. Cold Spring Harb Perspect Med. 2012;2:a006338.
14. Grunwald IC, Korte M, Wolfer D, Wilkinson GA, Unsicker K, Lipp HP, et al. Kinase-independent requirement of EphB2 receptors in hippocampal synaptic plasticity. Neuron. 2001;32:1027–40.
15. Cisse M, Halabisky B, Harris J, Devidze N, Dubal DB, Sun B, et al. Reversing EphB2 depletion rescues cognitive functions in Alzheimer model. Nature. 2011;469:47–52.
16. Bodin R, Paille V, Oullier T, Durand T, Aubert P, Le Berre-Scoul C, et al. The ephrin receptor EphB2 regulates the connectivity and activity of enteric neurons. J Biol Chem. 2021;297:101300.
17. Fagundes RR, Belt SC, Bakker BM, Dijkstra G, Harmsen HJM, Faber KN. Beyond butyrate: microbial fiber metabolism supporting colonic epithelial homeostasis. Trends Microbiol. 2024;32:178–89.
18. Sun J, Yuan B, Wu Y, Gong Y, Guo W, Fu S, et al. Sodium butyrate protects N2a cells against abeta toxicity in vitro. Mediators Inflamm. 2020;2020:7605160.
19. Jiang Y, Li K, Li X, Xu L, Yang Z. Sodium butyrate ameliorates the impairment of synaptic plasticity by inhibiting the neuroinflammation in 5XFAD mice. Chem Biol Interact. 2021;341:109452.
20. Fernando W, Martins IJ, Morici M, Bharadwaj P, Rainey-Smith SR, Lim WLF, et al. Sodium butyrate reduces brain amyloid-beta levels and improves cognitive memory performance in an Alzheimer's disease transgenic mouse model at an early disease stage. J Alzheimers Dis. 2020;74:91–9.
21. Butterfield DA, Poon HF. The senescence-accelerated prone mouse (SAMP8): a model of age-related cognitive decline with relevance to alterations of the gene expression and protein abnormalities in Alzheimer's disease. Exp Gerontol. 2005;40:774–83.
22. Hsiao K, Chapman P, Nilsen S, Eckman C, Harigaya Y, Younkin S, et al. Correlative memory deficits, Abeta elevation, and amyloid plaques in transgenic mice. Science. 1996;274:99–102.
23. Gao L, Davies DL, Asatryan L. Sodium butyrate supplementation modulates neuroinflammatory response aggravated by antibiotic treatment in a mouse model of binge-like ethanol drinking. Int J Mol Sci. 2022;23:15688.
24. Chevalier J, Derkinderen P, Gomes P, Thinard R, Naveilhan P, Vanden Berghe P, et al. Activity-dependent regulation of tyrosine hydroxylase expression in the enteric nervous system. J Physiol. 2008;586:1963–75.
25. Caillaud M, Le Drean ME, De-Guilhem-de-Lataillade A, Le Berre-Scoul C, Montnach J, Nedellec S, et al. A functional network of highly pure enteric neurons in a dish. Front Neurosci. 2022;16:1062253.
26. Van Landeghem L, Chevalier J, Mahe MM, Wedel T, Urvil P, Derkinderen P, et al. Enteric glia promote intestinal mucosal healing via activation of focal adhesion kinase and release of proEGF. Am J Physiol Gastrointest Liver Physiol. 2011;300:G976–87.
27. Stine WB, Jungbauer L, Yu C, LaDu MJ. Preparing synthetic Abeta in different aggregation states. Methods Mol Biol. 2011;670:13–32.
28. Workman MJ, Mahe MM, Trisno S, Poling HM, Watson CL, Sundaram N, et al. Engineered human pluripotent-stem-cell-derived intestinal tissues with a functional enteric nervous system. Nat Med. 2017;23:49–59.
29. Jarry A, Bossard C, Bou-Hanna C, Masson D, Espaze E, Denis MG, et al. Mucosal IL-10 and TGF-beta play crucial roles in preventing LPS-driven, IFN-gamma-mediated epithelial damage in human colon explants. J Clin Invest. 2008;118:1132–42.
30. Sanders KM, Koh SD, Ro S, Ward SM. Regulation of gastrointestinal motility-insights from smooth muscle biology. Nat Rev Gastroenterol Hepatol. 2012;9:633–45.
31. Jin J, Xu Z, Zhang L, Zhang C, Zhao X, Mao Y, et al. Gut-derived beta-amyloid: Likely a centerpiece of the gut-brain axis contributing to Alzheimer's pathogenesis. Gut Microbes. 2023;15:2167172.
32. Hampel H, Vassar R, De Strooper B, Hardy J, Willem M, Singh N, et al. The beta-Secretase BACE1 in Alzheimer's Disease. Biol Psychiatry. 2021;89:745–56.
33. Zhang X, Song W. The role of APP and BACE1 trafficking in APP processing and amyloid-beta generation. Alzheimers Res Ther. 2013;5:46.
34. El-Amouri SS, Zhu H, Yu J, Marr R, Verma IM, Kindy MS. Neprilysin: an enzyme candidate to slow the progression of Alzheimer's disease. Am J Pathol. 2008;172:1342–54.
35. Canani RB, Costanzo MD, Leone L, Pedata M, Meli R, Calignano A. Potential beneficial effects of butyrate in intestinal and extraintestinal diseases. World J Gastroenterol. 2011;17:1519–28.
36. Ulbricht W. Effects of veratridine on sodium currents and fluxes. Rev Physiol Biochem Pharmacol. 1998;133:1–54.
37. Han X, Tang S, Dong L, Song L, Dong Y, Wang Y, et al. Loss of nitrergic and cholinergic neurons in the enteric nervous system of APP/PS1 transgenic mouse model. Neurosci Lett. 2017;642:59–65.
38. Manocha GD, Floden AM, Miller NM, Smith AJ, Nagamoto-Combs K, Saito T, et al. Temporal progression of Alzheimer's disease in brains and intestines of transgenic mice. Neurobiol Aging. 2019;81:166–76.
39. Zhang R, Lu J, Pei G, Huang S. Galangin rescues Alzheimer's amyloid-beta induced mitophagy and brain organoid growth impairment. Int J Mol Sci. 2023;24:3398.
40. Randall KJ, Turton J, Foster JR. Explant culture of gastrointestinal tissue: a review of methods and applications. Cell Biol Toxicol. 2011;27:267–84.
41. Neunlist M, Toumi F, Oreschkova T, Denis M, Leborgne J, Laboisse CL, et al. Human ENS regulates the intestinal epithelial barrier permeability and a tight junction-associated protein ZO-1 via VIPergic pathways. Am J Physiol Gastrointest Liver Physiol. 2003;285:G1028–36.
42. Soret R, Chevalier J, De Coppet P, Poupeau G, Derkinderen P, Segain JP, et al. Short-chain fatty acids regulate the enteric neurons and control gastrointestinal motility in rats. Gastroenterology. 2010;138:1772–82.
43. Cuff MA, Lambert DW, Shirazi-Beechey SP. Substrate-induced regulation of the human colonic monocarboxylate transporter, MCT1. J Physiol. 2002;539:361–71.
44. Borthakur A, Saksena S, Gill RK, Alrefai WA, Ramaswamy K, Dudeja PK. Regulation of monocarboxylate transporter 1 (MCT1) promoter by butyrate in human intestinal epithelial cells: involvement of NF-kappaB pathway. J Cell Biochem. 2008;103:1452–63.
45. Suply E, de Vries P, Soret R, Cossais F, Neunlist M. Butyrate enemas enhance both cholinergic and nitrergic phenotype of myenteric neurons and neuromuscular transmission in newborn rat colon. Am J Physiol Gastrointest Liver Physiol. 2012;302:G1373–80.
46. Neunlist M, Rolli-Derkinderen M, Latorre R, Van Landeghem L, Coron E, Derkinderen P, et al. Enteric glial cells: recent developments and future directions. Gastroenterology. 2014;147:1230–7.
47. Clairembault T, Kamphuis W, Leclair-Visonneau L, Rolli-Derkinderen M, Coron E, Neunlist M, et al. Enteric GFAP expression and phosphorylation in Parkinson's disease. J Neurochem. 2014;130:805–15.
48. Yang T, Li S, Xu H, Walsh DM, Selkoe DJ. Large soluble oligomers of amyloid beta-protein from Alzheimer brain are far less neuroactive than the smaller oligomers to which they dissociate. J Neurosci. 2017;37:152–63.
49. Pan XD, Zhu YG, Lin N, Zhang J, Ye QY, Huang HP, et al. Microglial phagocytosis induced by fibrillar beta-amyloid is attenuated by oligomeric beta-amyloid: implications for Alzheimer's disease. Mol Neurodegener. 2011;6:45.

50. Colangelo AM, Alberghina L, Papa M. Astrogliosis as a therapeutic target for neurodegenerative diseases. Neurosci Lett. 2014;565:59–64.
51. Carter SF, Scholl M, Almkvist O, Wall A, Engler H, Langstrom B, et al. Evidence for astrocytosis in prodromal Alzheimer disease provided by 11C-deuterium-L-deprenyl: a multitracer PET paradigm combining 11C-Pittsburgh compound B and 18F-FDG. J Nucl Med. 2012;53:37–46.
52. Morley JE, Armbrecht HJ, Farr SA, Kumar VB. The senescence accelerated mouse (SAMP8) as a model for oxidative stress and Alzheimer's disease. Biochim Biophys Acta. 2012;1822:650–6.
53. Hao MM, Foong JP, Bornstein JC, Li ZL, Vanden Berghe P, Boesmans W. Enteric nervous system assembly: Functional integration within the developing gut. Dev Biol. 2016;417:168–81.
54. Pacesova A, Holubova M, Hruba L, Strnadova V, Neprasova B, Pelantova H, et al. Age-related metabolic and neurodegenerative changes in SAMP8 mice. Aging. 2022;14:7300–27.
55. Pellegrini C, Daniele S, Antonioli L, Benvenuti L, D'Antongiovanni V, Piccarducci R, et al. Prodromal intestinal events in Alzheimer's Disease (AD): colonic dysmotility and inflammation are associated with enteric AD-related protein deposition. Int J Mol Sci. 2020;21:3523.
56. Fernandez A, Quintana E, Velasco P, Moreno-Jimenez B, de Andres B, Gaspar ML, et al. Senescent accelerated prone 8 (SAMP8) mice as a model of age dependent neuroinflammation. J Neuroinflammation. 2021;18:75.
57. Liu G, Yu Q, Zhu H, Tan B, Yu H, Li X, et al. Amyloid-beta mediates intestinal dysfunction and enteric neurons loss in Alzheimer's disease transgenic mouse. Cell Mol Life Sci. 2023;80:351.
58. Miners JS, Van Helmond Z, Chalmers K, Wilcock G, Love S, Kehoe PG. Decreased expression and activity of neprilysin in Alzheimer disease are associated with cerebral amyloid angiopathy. J Neuropathol Exp Neurol. 2006;65:1012–21.
59. Chen C, Ahn EH, Kang SS, Liu X, Alam A, Ye K. Gut dysbiosis contributes to amyloid pathology, associated with C/EBPbeta/AEP signaling activation in Alzheimer's disease mouse model. Sci Adv. 2020;6:eaba0466.
60. Qu C, Xu QQ, Yang W, Zhong M, Yuan Q, Xian YF, et al. Gut dysbiosis aggravates cognitive deficits, amyloid pathology and lipid metabolism dysregulation in a transgenic mouse model of Alzheimer's disease. J Pharm Anal. 2023;13:1526–47.
61. Zhang Y, Shen Y, Liufu N, Liu L, Li W, Shi Z, et al. Transmission of Alzheimer's disease-associated microbiota dysbiosis and its impact on cognitive function: evidence from mouse models and human patients. Mol Psychiatry. 2023;28:4421–37.
62. Qian XH, Xie RY, Liu XL, Chen SD, Tang HD. Mechanisms of short-chain fatty acids derived from gut microbiota in Alzheimer's disease. Aging Dis. 2022;13:1252–66.
63. Marizzoni M, Cattaneo A, Mirabelli P, Festari C, Lopizzo N, Nicolosi V, et al. Short-chain fatty acids and lipopolysaccharide as mediators between gut dysbiosis and amyloid pathology in Alzheimer's disease. J Alzheimers Dis. 2020;78:683–97.
64. Sampson TR, Challis C, Jain N, Moiseyenko A, Ladinsky MS, Shastri GG, et al. A gut bacterial amyloid promotes alpha-synuclein aggregation and motor impairment in mice. eLife. 2020;9:e53111.
65. Miller AL, Bessho S, Grando K, Tukel C. Microbiome or infections: amyloid-containing biofilms as a trigger for complex human diseases. Front Immunol. 2021;12:638867.
66. Hu R, Wei P, Jin L, Zheng T, Chen WY, Liu XY, et al. Overexpression of EphB2 in hippocampus rescues impaired NMDA receptors trafficking and cognitive dysfunction in Alzheimer model. Cell Death Dis. 2017;8:e2717.
67. Spencer NJ, Costa M, Hibberd TJ, Wood JD. Advances in colonic motor complexes in mice. Am J Physiol Gastrointest Liver Physiol. 2021;320:G12–29.
68. Miyamoto T, Kim D, Knox JA, Johnson E, Mucke L. Increasing the receptor tyrosine kinase EphB2 prevents amyloid-beta-induced depletion of cell surface glutamate receptors by a mechanism that requires the PDZ-binding motif of EphB2 and neuronal activity. J Biol Chem. 2016;291:1719–34.
69. Shi XD, Sun K, Hu R, Liu XY, Hu QM, Sun XY, et al. Blocking the interaction between EphB2 and ADDLs by a small peptide rescues impaired synaptic plasticity and memory deficits in a mouse model of Alzheimer's disease. J Neurosci. 2016;36:11959–73.
70. O'Malley D, Liston M, Hyland NP, Dinan TG, Cryan JF. Colonic soluble mediators from the maternal separation model of irritable bowel syndrome activate submucosal neurons via an interleukin-6-dependent mechanism. Am J Physiol Gastrointest Liver Physiol. 2011;300:G241–52.
71. Cresci GA, Thangaraju M, Mellinger JD, Liu K, Ganapathy V. Colonic gene expression in conventional and germ-free mice with a focus on the butyrate receptor GPR109A and the butyrate transporter SLC5A8. J Gastrointest Surg. 2010;14:449–61.
72. Vagnerova K, Hudcovic T, Vodicka M, Ergang P, Klusonova P, Petr Hermanova P, et al. The effect of oral butyrate on colonic short-chain fatty acid transporters and receptors depends on microbial status. Front Pharmacol. 2024;15:1341333.
73. Dalile B, Van Oudenhove L, Vervliet B, Verbeke K. The role of short-chain fatty acids in microbiota-gut-brain communication. Nat Rev Gastroenterol Hepatol. 2019;16:461–78.
74. Wang C, Zheng D, Weng F, Jin Y, He L. Sodium butyrate ameliorates the cognitive impairment of Alzheimer's disease by regulating the metabolism of astrocytes. Psychopharmacology (Berl). 2022;239:215–27.
75. Hall CM, Lasli S, Serwinski B, Djordjevic B, Sheridan GK, Moeendarbary E. Hippocampus of the APP(NL-G-F) mouse model of Alzheimer's disease exhibits region-specific tissue softening concomitant with elevated astrogliosis. Front Aging Neurosci. 2023;15:1212212.
76. Gonzalez-Rodriguez M, Villar-Conde S, Astillero-Lopez V, Villanueva-Anguita P, Ubeda-Banon I, Flores-Cuadrado A, et al. Neurodegeneration and astrogliosis in the human CA1 hippocampal subfield are related to hsp90ab1 and bag3 in Alzheimer's disease. Int J Mol Sci. 2021;23:165.
77. Govindarajan N, Agis-Balboa RC, Walter J, Sananbenesi F, Fischer A. Sodium butyrate improves memory function in an Alzheimer's disease mouse model when administered at an advanced stage of disease progression. J Alzheimers Dis. 2011;26:187–97.

ACKNOWLEDGEMENTS

This work was supported by the Institut National de la Santé et de la Recherche Médicale (INSERM), the Nantes Université, the Institut National de Recherche pour l'Agriculture, l'Alimentation et l'Environnement (INRAE) and ANR (Grant No. 24-CE14-7354 to MC). We are grateful to Pays de la Loire for their financial support through the interregional project PROLIFIC (2019-013227 to MN). We thank Laure Verret and Université Toulouse III - Paul Sabatier Centre de Biologie Intégrative Centre de Recherches sur la Cognition Animale - CNRS UMR 5169 for providing us with colon tissues of Tg2576 mice. We thank Pierre-Etienne Sado for administrative help. We thank Tony Durand for assistance in designing RT-qPCR primers. We thank Katy Fontaine and Karelle Smadja for administrative assistance.

AUTHOR CONTRIBUTIONS

MC, MN and RB conceived and planned this study. RB, MN, VP, PN, MCa, MM, TO, LB, HF, Y-L, PA and MC contributed to supervising experimental design. VP, TO, AB, GD, LB, AB, PA and RB conducted the experiments. RB, TO, VP, MCa, SP, LV, GD and MC performed collection of the data and statistical analysis. RB, MN and MC wrote the manuscript. All authors reviewed and approved of the manuscript.

COMPETING INTERESTS

The authors declare no competing interests.

ADDITIONAL INFORMATION

Supplementary information The online version contains supplementary material available at https://doi.org/10.1038/s41380-026-03522-6.

Correspondence and requests for materials should be addressed to Moustapha Cissé.

Reprints and permission information is available at http://www.nature.com/reprints

Publisher's note Springer Nature remains neutral with regard to jurisdictional claims in published maps and institutional affiliations.